

Elisabeth Löfsved, Bengt Lundborg, Peter Holm, Åsa Waern

## **Deterministic calculation of wave propagation in urban areas**





SWEDISH DEFENCE RESEARCH AGENCY  
Command and Control Systems  
P.O. Box 1165  
SE-581 11 Linköping

FOI-R--1339--SE

September 2004

ISSN 1650-1942

**Methodology report**

Elisabeth Löfsved, Bengt Lundborg, Peter Holm, Åsa Waern

# **Deterministic calculation of wave propagation in urban areas**



<b>Issuing organization</b> FOI – Swedish Defence Research Agency Command and Control Systems P.O. Box 1165 SE-581 11 Linköping	<b>Report number, ISRN</b> FOI-R--1339--SE	<b>Report type</b> Methodology report
	<b>Research area code</b> 4. C4ISTAR	
	<b>Month year</b> September 2004	<b>Project no.</b> E7063
	<b>Sub area code</b> 41 C4I	
	<b>Sub area code 2</b>	
<b>Author/s (editor/s)</b> Elisabeth Löfsved Bengt Lundborg Peter Holm Åsa Waern	<b>Project manager</b> Åsa Waern	
	<b>Approved by</b> Sören Eriksson	
	<b>Sponsoring agency</b> Armed Forces Headquarter, Sweden	
	<b>Scientifically and technically responsible</b> Bengt Lundborg	
<b>Report title</b> Deterministic calculation of wave propagation in urban areas		
<b>Abstract (not more than 200 words)</b>  Urban environment is an unexplored field of knowledge for military radio communication. There is an increasing need for understanding radio wave propagation, and how to model it, in urban terrain. The frequent lack of line-of-sight between a transmitter and a receiver means that the radio waves mostly have to propagate by diffraction over roof tops and around house corners. Radio waves will also be reflected and scattered by obstacles of different sizes and textures.  FOI has acquired computer software called <i>Radiowave Propagation Simulator (RPS)</i> , which was considered appropriately general and flexible. It is originally designed for coverage planning of cellular radio systems. This report describes how we studied the handling of the software and its usability for outdoor scenarios, which differ a lot from the original intended usage. We have compared simulated data to measurements made in Stockholm.  We have found that it is complicated to design a correct enough model and to validate it by measurements. Still, the commercial software, that allows custom plug-ins, is considered a cost effective tool that can be recommended for future radio wave propagation calculations.		
<b>Keywords</b> Wave propagation, urban environment, RPS, geometrical optics, ray tracing		
<b>Further bibliographic information</b>	<b>Language</b> English	
<b>ISSN</b> 1650-1942	<b>Pages</b> 64 p.	
	<b>Price acc. to pricelist</b>	

<b>Utgivare</b> Totalförsvarets Forskningsinstitut - FOI Ledningssystem Box 1165 581 11 Linköping	<b>Rapportnummer, ISRN</b> FOI-R--1339--SE	<b>Klassificering</b> Metodrapport
	<b>Forskningsområde</b> 4. Ledning, informationsteknik och sensorer	
	<b>Månad, år</b> September 2004	<b>Projektnummer</b> E7063
	<b>Delområde</b> 41 Ledning med samband, telekom och IT-system	
	<b>Delområde 2</b>	
<b>Författare/redaktör</b> Elisabeth Löfsved Bengt Lundborg Peter Holm Åsa Waern	<b>Projektledare</b> Åsa Waern	
	<b>Godkänd av</b> Sören Eriksson	
	<b>Uppdragsgivare/kundbeteckning</b> Försvarsmakten, HKV	
	<b>Tekniskt och/eller vetenskapligt ansvarig</b> Bengt Lundborg	
<b>Rapportens titel (i översättning)</b> Deterministisk beräkning av vågutbredning i stadsmiljö		
<b>Sammanfattning (högst 200 ord)</b>  Stadsmiljö är ett utforskat område vad det gäller militär radiokommunikation. Detta leder till ett ökat behov av förståelsen för radiovågors utbredning och hur de skall modelleras i stadsmiljö. Då sträckor med direkt belysning ofta saknas leder det till att radiovågen bara kan nå mottagaren genom att diffraktera över hustak och runt hörn. Vågorna kommer även att reflekteras och spridas av ytor av varierande storlek.  FOI har köpt in en programvara utvecklad för beräkningar av radiovågors utbredning i stadsmiljö. Programmet RPS (Radiowave Propagation Simulator) valdes för dess generalitet och flexibilitet. I denna rapport studeras hanteringen av programvaran och dess användbarhet för utomhusscenarien som skiljer sig ganska mycket från vad programmet designats för. Vi har gjort jämförelser mellan simuleringar och mätningar som gjorts i Stockholm.		
Vi har erfart att en korrekt beräkningsmodell är komplicerad både att utveckla och validera. Därför anser vi att den inhandlade programvaran, som tillåter egentillverkade moduler, är ett kostnadseffektivt verktyg som kan användas för framtida behov av vågutbredningsberäkningar.		
<b>Nyckelord</b> Vågutbredning, stadsmiljö, RPS, geometrisk optik, strålberäkningar		
<b>Övriga bibliografiska uppgifter</b>		<b>Språk</b> Engelska
<b>ISSN</b> 1650-1942		<b>Antal sidor:</b> 64 s.
<b>Distribution enligt missiv</b>		<b>Pris:</b> Enligt prislista

# Table of Contents

Table of Contents .....	5
Chapter 1 Introduction .....	7
1.1. Background .....	7
1.2. Outline of the report.....	7
1.3. Scope of the investigation.....	8
Chapter 2 Wave propagation in urban areas .....	9
2.1. Propagation models .....	10
Chapter 3 The RPS software.....	16
3.1. Basic facts on RPS.....	16
3.2. Static simulation presentation.....	17
3.3. Dynamic simulations .....	20
3.4. Import/Export of data.....	23
3.5. Material properties .....	24
3.6. Ray tracing.....	26
3.7. Empirical model.....	28
3.8. Antennas.....	29
3.9. Experiences of RPS and tests.....	32
Chapter 4 Comparison RPS vs. Stockholm measurements.....	34
4.1. Wideband measurements .....	37
4.1.1 Measurement setup .....	37
4.1.2 Simulations.....	38
4.2. Narrowband measurements.....	39
4.2.1 Simulation Setup.....	40
4.2.2 Comparison.....	41
Chapter 5 Scenario Aerostat .....	44
5.1. Description of the scenario.....	44
5.2. Results of the calculations.....	46
5.3. Discussion .....	48
Chapter 6 Conclusions.....	51
6.1. Future Work.....	51
Chapter 7 References .....	53
Appendix A Export of data.....	55
Appendix B Narrowband results, Stockholm.....	58



# Chapter 1 Introduction

## 1.1. Background

Urban warfare is likely to be a more and more common task for armed forces. Also Swedish participation abroad in peace-keeping, peace-enforcement and battle will be more common. The Urban environment sets limitations on communication systems. The lack of line-of-sight propagation means that the radio waves can reach the receiver via diffraction over rooftops and around corners. Furthermore, the waves will reflect against and scatter at, not only big objects, like walls and asphalt surfaces, but also cars parked in the street, lamp posts and traffic signs. The amount of reflections and scattering depends on the frequency, angle of arrival and the surface material. This gives rise to multipath propagation and high attenuation, which may result in disturbances and interruptions in the transmission.

In many ways the communication scenarios may differ from those of peacetime civilian telecom, e.g. with respect to frequencies and waveforms used, locations of terminal antennas, possible base station infrastructure and interference and jamming environment. As a consequence, there is an increasing need for understanding and modelling the radio wave propagation in urban terrain with particular focus on the military scenarios.

FOI has a contract with the Armed Forces Headquarters to investigate the radio channel properties in urban military scenarios. To this end FOI has acquired computer software developed for radio wave propagation calculation in urban environments. One major advantage by using commercial software is that the cost and time to develop such software may be prohibitive. There are several such softwares on the market. We have chosen the program Radio Propagation Simulator (RPS) from Radioplan, Germany, because of its generality and flexibility. In particular, it allows custom plug-ins, which may become necessary to modify calculation algorithms to lower frequencies. According to Radioplan, the frequency range for the software is 300 MHz to 300 GHz. Military radio systems use even lower frequencies and a frequency range down to 50 MHz is of interest.

## 1.2. Outline of the report

Chapter 2 introduces wave propagation in urban areas and some deterministic and semi-deterministic and empirical models.

Chapter 3 describes the Radiowave Propagation Simulator software, RPS, in general. The following components are described a bit further: simulation result presentations, dynamic simulations, import/export of data, material properties, ray tracing, antennas. The chapter finishes with a presentation of some experiences and tests of the software.

Chapter 4 contains comparisons between simulation results and measurements. The two sets of measurements are described as well as the simulation set up for respective scenario.

Chapter 5 describes a test calculation for an elevated transmitter carried by an aerostat placed over Gärde in Stockholm.

Chapter 6 contains the general conclusions of our work with RPS and ideas of future work.

Chapter 7 contains the references.

### **1.3. Scope of the investigation**

From the beginning of the work with this report we decided only to work with outdoor scenarios. In all the simulations we have not allowed penetration through the buildings, since this gives much higher simulation times. The simulations are made with the setup described before each simulation scenario and are chosen to give results for most of the points in the grid of receivers and not to have too long simulation times. We have seen that the results are very sensitive to the settings as is illustrated in section 3.9. The scenarios investigated in chapters 4 and 5 were calculated with settings that gave sufficient number of rays, but the effects of different settings were not investigated separately.

During the work we successively learnt more about the composition of the different calculations performed in RPS and strategies for the program settings. The RPS calculations are very time-consuming and therefore, unfortunately, we have not been able to rerun them to account for our new knowledge. Hence the results given in the report are sometimes far from optimal.

The software supports long simulations, but when parallelizing the simulations using workstations in use by others, it has happened the simulation accidentally has been stopped by some user and then the simulation has had to be started over from the beginning. This has sometimes been a problem. At present there is also a problem with load sharing in parallelized computations. The rays are distributed initially between the processors. This load should be redistributed dynamically when a processor has finished its given task. This does not happen and because of this the expected substantial gain in processing speed with several computers is never obtained.

## Chapter 2 Wave propagation in urban areas

In urban environment, the lack of line-of-sight propagation forces the radio waves to diffract over rooftops and around corners. The waves will reflect against and scatter at different obstacles. The amount of reflections and scattering depends on the frequency, angle of arrival and the surface material. This results in multipath propagation i.e. the signals reach the receiver from different paths. The paths followed by the individual waves have different lengths. The total received signal is the coherent sum of the individual signals arriving with their different phases. A phenomenon that then occurs is called fast fading or small-scale fading i.e. rapid fluctuations of the received signal strength. The variations can be as much as 40 dB.

Due to the different path lengths, the multipath components do not reach the receiver at the same time, producing time dispersion of the received signals. A harmful possible consequence of this is intersymbol interference.

Path loss or propagation loss is the parameter commonly used to characterize the local average signal in mobile channels. It is defined as the relationship between the transmitted power of the transmitter antenna and the received power by the receiver antenna. In most cases, path loss is expressed in dB.

Another parameter used to characterize the mobile propagation channel is the local average receiver signal. This is obtained by averaging the received signal over tracks of several wavelength or small areas with a radius of several wavelengths. When the receiver moves along a trajectory, the local average signal suffers fluctuations known as slow fading or large-scale signal variations. These variations of the local average are a consequence of the attenuation of the signal with the distance between the transmitter and receiver and the presence of the obstacles in the environment. The rate of the slow fading variations is of the order of the size of the obstacles surrounding the receiver. Therefore, in rural environments, the local average shows a smoother variation than in urban scenarios.

Models that calculate the wave propagation can be divided in three different classes [Cátedra and Pérez-Arriaga, 1999]:

- Empirical models
- Semiempirical or semideterministic models
- Deterministic models

The empirical models are described by equations derived from statistical analysis of a large number of measurements. These methods are simple and fast to apply. They cannot, though, provide any accurate estimation because of their simplicity.

The deterministic models are based on the application of well-known electromagnetic techniques to a site-specific description of the environments. The environmental description is obtained from building and terrain databases. Most of the deterministic models are based on ray-tracing electromagnetic methods.

Semiempirical or semideterministic models are based on the equations derived from the application of deterministic methods to generic urban or indoor models. Sometimes, the equations have

been corrected experimentally in order to improve their agreement with the measurements. These methods require more detailed information about the environment than the empirical methods but not as much as the deterministic models.

Beside the three different classes above, the propagation models can be classified according to the scenario to which they are applied. Three generic categories of environments (cells) can be considered:

- Macrocells; which are large areas, of radius between 1 and 30 km from the transmitter, and with the transmitter antenna well above the surrounding buildings.
- Microcells; which occupy smaller areas with a radius between 0.1 and 1 km from the transmitter. The transmitter antenna can be above, below or at the same level as the surrounding buildings.
- Picocells; which occupy a radius between 0.01 and 0.1 km. There are two types of picocells: indoor and outdoor. The transmitter antenna is below the rooftop level or inside a building.

Several articles about radio wave propagation in built-up areas can be found. However, in many of these, the ray tracing problem is reduced to a minimum by idealizing the building geometry of an urban area. In [Walfisch and Bertoni, 1988], [Saunders and Bonar, 1991], [Neve and Rowe, 1994], and [Juan-Llácer and Cardona, 1997], an urban area is idealized as a row of knife edges of equal heights and spacings or as a row of houses of equal widths, heights, and spacings. Here, the problem is reduced to calculation of a multiple-diffracted field in two dimensions. Also, articles can be found where the problem is reduced to calculation of multiple-reflected fields in two dimensions by assuming houses with infinite heights. There are very few good articles that deal with propagation in urban environments using both reflected and diffracted rays in three dimensions. Attempts using an idealized building geometry can be found in [Blaunstein and Levin, 1996], [Tan and Tan, 1996], and [Kanatas et al., 1997], for instance. The reason is, of course, that the problem is very complex. Because of that, still, simplified models like Okumura-Hata and Walfisch-Ikegami described below are used.

## 2.1. Propagation models

### Okumura-Hata Model

The Okumura-Hata model [Cátedra and Pérez-Arriaga, 1999] is a macrocell empirical model developed from measurements made in Tokyo at the frequencies of 150, 450 and 900 MHz. The model provides closed expressions for the median path loss for different environments. For urban environment, the median path loss is:

$$L_u = 69.55 + 26.16 \log f - 13.82 \log h_t - a(h_m) + (44.9 - 6.55 \log h_t) \log d$$

where

$f$  = frequency in the range  $150 \text{ MHz} \leq f \leq 1500 \text{ MHz}$

$h_t$  = effective transmitter antenna (Tx) height in the range  $30 \text{ m} \leq h_t \leq 200 \text{ m}$

$h_m$  = receiver antenna (Rx) height in the range  $1 \text{ m} \leq h_m \leq 10 \text{ m}$

$d$  = distance between Tx and Rx in the range  $1 \text{ km} \leq d \leq 20 \text{ km}$

The term  $a(h_m)$  is a correction factor. For small and medium-sized cities it is given by:

$$a(h_m) = (1.1 \log f - 0.7)h_m - (1.56 \log f - 0.8)$$

For large cities:

$$\begin{aligned} a(h_m) &= 8.29(\log 1.54h_m)^2 - 1.1 && \text{when } f \leq 300 \text{ MHz} \\ a(h_m) &= 3.2(\log 11.75h_m)^2 - 4.97 && \text{when } f \geq 300 \text{ MHz} \end{aligned}$$

This model works adequately for large cell mobile systems but not for cells with a radius of the order of 1 km.

### COST 231 - Hata model

The COST 231 Hata model [Cátedra and Pérez-Arriaga, 1999] is a modification of the Okumura-Hata model for European cities and the frequency range 1500 – 2000 MHz. The path loss is given by:

$$L_u = 46.3 + 33.9 \log f - 1.82 \log h_t - a(h_m) + (44.9 - 6.55 \log h_t) \log d + C_M$$

where  $C_M = 3$  dB in metropolitan centres and 0 dB otherwise.

The range for the other parameters is the same as in the Hata model.

### Walfisch and Bertoni model

This is a macrocell semideterministic model [Cátedra and Pérez-Arriaga, 1999] suitable for homogeneous urban and suburban areas. The propagation equations are derived from an ideal model of a city where the buildings are organized such that they form parallel rows with uniform height and width. The model is valid when there is a non-line-of-sight situation between the base station and the receiver. The path loss is estimated as:

$$L = 89.55 + 21 \log f + 38 \log d - 18 \log H + A - 18 \log \left( 1 - \frac{d^2}{17H} \right)$$

where

$f$  = frequency in MHz

$d$  = distance transmitter - receiver, in km

$H$  = average height of the transmitter antenna with respect to the surrounding building

$A$  = models the influence of the buildings:

$$A = 5 \log \left[ \left( \frac{b}{2} \right)^2 + (h_B - h_m)^2 \right] - 9 \log b + 20 \log \left\{ \operatorname{tg}^{-1} \left[ \frac{2(h_B - h_m)}{b} \right] \right\}$$

where

$h_B$  = is the building heights, in meters

$h_m$  = receiver antenna (Rx) height in meters

$b$  = is the row spacing

The model requires that the transmitter antenna is above the rooftop level.

## COST 231-Walfisch-Ikegami model

This is a macrocell semideterministic model suitable for urban environments, [Cátedra and Pérez-Arriaga, 1999]. It is based on the Walfisch-Bertoni and Ikegami models. There are no restrictions on the position of the transmitter antenna with respect to the rooftop level. The path loss is calculated as the sum of three terms:

$$L = L_0 + L_1 + L_2$$

The first term  $L_0$  is the free space loss for isotropic antennas:

$$L_0 = 10 \log \frac{(4\pi d)^2}{\lambda^2}$$

The second term is:

$$L_1 = -16.9 - 10 \log w + 10 \log f + 20 \log(h_R - h_m) + L_{11}(\phi)$$

where

$w$  = is the width of the street where the receiver is, in meters

$f$  = frequency,  $800 \text{ MHz} \leq f \leq 2000 \text{ MHz}$

$d$  = distance between transmitter and receiver antennas,  $0.02 \text{ km} \leq r \leq 5 \text{ km}$

$h_R$  = is the average building heights, in meters

$h_m$  = receiver antenna (Rx) height in meters,  $1 \text{ m} \leq h_m \leq 3 \text{ m}$

and

$$L_{11}(\phi) = \begin{cases} -10 + 0.3571\phi & 0 < \phi < 35^\circ \\ 2.5 + 0.075(\phi - 35^\circ) & 35^\circ \leq \phi < 55^\circ \\ 4 - 0.1114(\phi - 55^\circ) & 55^\circ \leq \phi \leq 90^\circ \end{cases}$$

with  $\phi$  being the angle formed by the street axis and the line connecting the transmitter and receiver antennas.

The third term is:

$$L_2 = L_{21} + k_a + k_d \log d + k_f \log f - 9 \log b$$

where

$$L_{21} = \begin{cases} -18 \log(1 + h_B - h_R), & h_B \geq h_R \\ 0, & h_B < h_R \end{cases}$$

$$k_a = \begin{cases} 54, & h_B \geq h_R \\ 54 - 0.8(h_B - h_R), & h_B < h_R \wedge d \geq 0.5 \text{ m} \\ 54 - 0.4d(h_B - h_R), & h_B < h_R \wedge d < 0.5 \text{ m} \end{cases}$$

$$k_d = \begin{cases} 18, & h_B \geq h_R \\ 18 - \frac{15(h_B - h_R)}{h_R}, & h_B < h_R \end{cases}$$

$$k_f = -4 + k_{f1} \left( \frac{f}{925} - 1 \right)$$

with

$h_B$  = being the transmitter antenna height,  $4 \text{ m} \leq h_B \leq 50 \text{ m}$

$b$  = the distance between the centres of adjacent rows of buildings

$k_{f1} = 1.5$  in metropolitan centres and 0.7 otherwise

The equations are valid for non-line-of-sight situations.

## GTD

GTD, the Geometrical Theory of Diffraction [McNamara et al., 1990], is a deterministic model commonly used in built-up areas. It is able to account for multi-path propagation in 3D and also back scattered rays, that is, propagation paths going backward. An example of a backscattered ray is the multiple reflected one in Figure 2.1.

GTD is an extension of the ray based method geometrical optics (GO). Besides reflected rays, GTD is able to account for diffracted rays. Both reflected and diffracted rays are calculated with

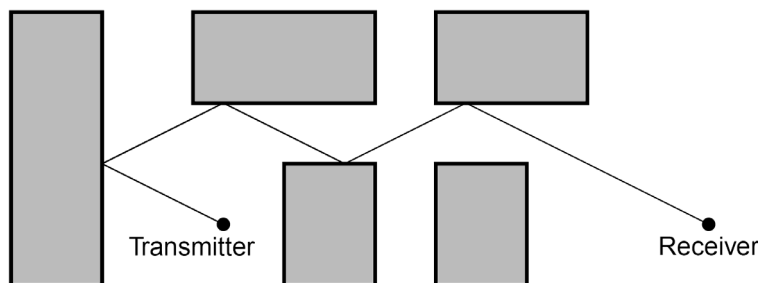


Figure 2.1. Example of a multiply reflected ray in an urban area. The ray is reflected by building walls in both forward and backward directions towards a receiver.

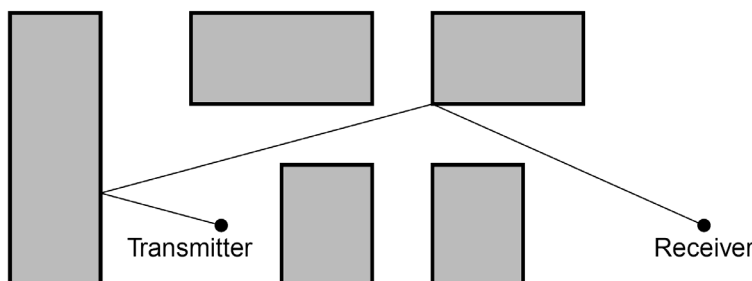


Figure 2.2. Example of a reflected and diffracted ray in an urban area.

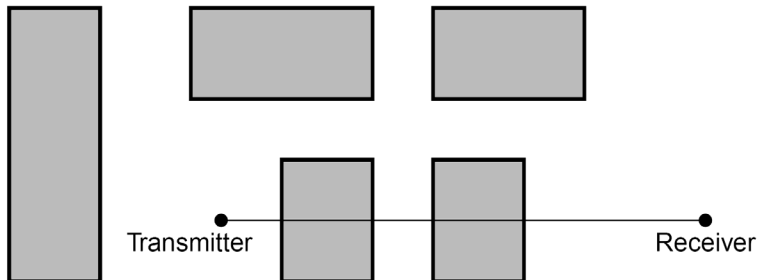


Figure 2.3. Example of a ray diffracted over roof tops towards a receiver in an urban area

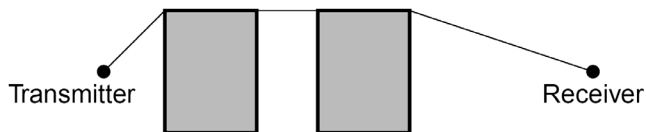


Figure 2.4. Example of a ray diffracted over two houses of equal heights and with flat roof tops. The ray is diffracted four times before it reaches the receiver.

correct phases and summed up. Also, a ray is allowed to be both reflected and diffracted before it arrives to the receiver. Figure 2.2 shows a ray first reflected by a wall and then diffracted by a vertical corner of a house.

In Figure 2.3, a ray is diffracted by roof tops. From above it is seen as one ray. But, in this case, it is also possible that more than one ray is involved. However, if the antennas are below rooftops and the houses are of equal height and have flat roofs, there is only one ray; see Figure 2.4. For houses with different heights, there can be more than one ray, especially if the antennas are above the roof heights. In Figure 2.5, we have three houses of different heights and with v-shaped roofs. For this simple diffraction geometry, there are 8 possible rays, that is, one direct ray,  $\binom{3}{1} = 3$  single-diffracted,  $\binom{3}{2} = 3$  double-diffracted, and  $\binom{3}{3} = 1$  triple-diffracted rays. Obviously, there can be quite a lot of rays to consider in an urban environment. Considering five houses instead of three, as shown in Figure 2.5, the worst case would be one direct ray plus  $\binom{5}{1} + \binom{5}{2} + \binom{5}{3} + \binom{5}{4} + \binom{5}{5} = 31$  diffracted rays, that is, a total of 32 rays. Adding to this also the possibility of reflections from walls and diffractions by vertical house corners, one can realize that the number of possible rays can be huge in an urban environment. Of course, not all of these rays will be important, that is, they will not all significantly contribute to the field strength.

One problem within ray based models is obviously to find important rays, or important propagation paths, connecting the transmitter with the receiver. Usually, a built-up area gives a huge number of possible rays to choose from, and one has to find the ones that contribute most to the field strength. For scenarios involving a large number of buildings, the implementation of an efficient routine, tracing important rays in three dimensions, is far from straightforward. On the other hand, when the task of finding important rays is done, the calculation of the field strength is quite straightforward. The Ray-tracing technique is further described in section 3.6.

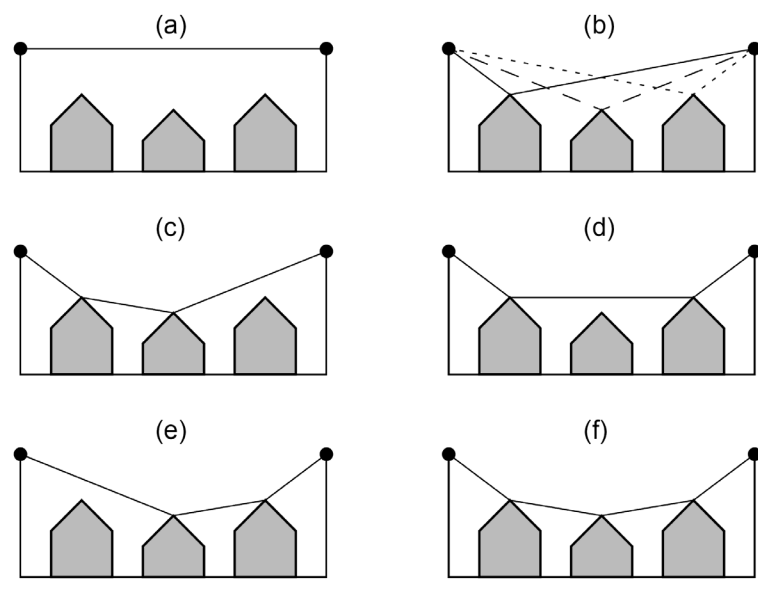


Figure 2.5. Diffraction by three v-shaped roof tops. In this example there are one direct ray, figure (a), three single-diffracted rays, figure (b), three double-diffracted rays, figures (c) to (e), and one triple-diffracted ray, figure (f).

# Chapter 3 The RPS software

RPS (Radio Propagation Simulator) is a software from Radioplan GmbH, Dresden, Germany. It is a radio coverage/performance planning system for radio systems. It comprises a wide band deterministic channel model for urban environments based on geometrical optics. All information regarding RPS in this chapter is based on the manuals for the used versions [RPS 5.1], [RPS 5.2], the software homepage [www.radioplan.com](http://www.radioplan.com) and the program code.

The software is chosen after comparison with some similar software's [Lundborg and Tronarp, 2003] for the reasons that it is general, flexible and fulfils our requirements. It supports simulations in the frequency range 300 MHz - 300 GHz. The software supports user-written modules. The program code is continuously further developed by Radioplan and their support has been excellent. The current version of the software supports parallelization of the simulations using several computers in the local network. This feature is of vital importance since the simulation times often are very long. It is very simple to start the parallelized simulations and it is possible to use computers running Windows or Linux operating systems.

To make simulations with the software the exterior (and interior) and material properties of each building in the environment must be described. This can conveniently be achieved by importing a building database of the supported formats and thereafter assign the material properties to the buildings. The material properties of the buildings are essential for how the wave propagation is calculated; they affect the reflection, diffraction and penetration of the signal. A database of material properties is enclosed with the program. But this only provides values for one frequency, and since the material properties are dependent on the frequency, a recalculation for all other frequencies has to be done.

When a simulation is accomplished there are a lot of presentation possibilities in RPS. Integrated in the program are plot functions for: coverage, best server, signal to interference ratio, delay spread and angular spread. There are also plug-ins which show other properties of the results and it is possible to make custom plug-ins. One of the advantages of making the presentations within RPS is that the simulation environment is shown simultaneously with the result. The results can be exported for use outside RPS, for example in Matlab.

For the description of the environment in which the simulations are to be made, a database of the buildings is needed. Such databases are produced by Lantmäteriverket and Metria for the use in telecommunication network planning. For the simulations in this report a database of Norrmalm in Stockholm is used. This database was not directly usable in RPS; as it only included the height and shape of the flat roofs of the buildings, we had to convert it to the format of object lists. There are two other supported database formats DWG and DXF. DXF means Drawing Exchange Format and is supported by many CAD applications, unfortunately there exist non-compatible dialects and thus often the database can not be used as is. We have had similar experiences of having to convert the data format when making tests on other softwares.

## 3.1. Basic facts on RPS

The frequency range for the software is 300 MHz to 300 GHz.

Ray tracing algorithms or the simpler empirical COST 231 models can be used for the simulation. The ray tracing algorithms are either 2.5D or 3D and the simulation is built up from reflections, diffractions and transmission through buildings. The ray tracing is further described in section 3.6.

The software contains a lot of plot functions for impulse responses and for the angle of arrival and departure of the signals. Ray paths and coverage plots can be shown in the propagation environment; these are further described in section 3.2.

Furthermore, data can be exported in ASCII text format or Matlab binary format, giving the possibility for the user to post process data. This gives a lot of opportunities for plotting whatever wanted. It is also possible to write Matlab-plug-ins to use for own defined presentations in RPS. The data export is further described in section 3.4 and in Appendix A.

Time variant impulse responses can be generated for quite complicated movements, defined by the user. The calculation is based on the static channel calculation of the field and thus the large scale effects can be seen. From the dynamic simulation it is possible to achieve long sequences of channel data which are not repeated. The dynamic simulation is further described in section 3.3.

### **3.2. Static simulation presentation**

A static simulation is a simulation with both transmitters and receivers at fix positions. At each receiver in the simulation environment it is possible to get an impulse response for each of the transmitters, if using ray tracing. Within the program each multipath component contributes to the signal strength at the receiver with the proper delay, which means, in principle, that the bandwidth is infinite. The static simulation can be used either for radio coverage/ performance planning for a system or it can be used as a base for dynamic simulations.

When the simulation is made, either via a ray tracing or empirical models, there are a lot of presentation possibilities of the simulation result in RPS. The five most used output presentations are integrated in the program and 16 more are pre-defined plug-ins. The integrated ones are further described later in this section. It is possible to define and write plug-ins of your own. One of the advantages of using RPS for the presentations is that the results are shown together with the propagation environment. It is also possible to export data to use with other programs. The export options are described in section 3.4. Another advantage of using RPS for the presentation is that within the program it is possible to view the propagation paths of the rays, if they are stored during the simulation; see Figure 3.1b). The result presentation in RPS also provides histograms of the surface plots. A path analysis can be calculated for an arbitrary section of the simulation which is covered with receivers. The path analysis then presents the received power and the delay spread either as a histogram or as a table. There are also three plug-ins which belong to the path analysis and can show the impulse response and the power angle profile at the respective transmitter and receiver.

The advantage of using Matlab for the presentation is that you can show precisely what you are interested in and that you know exactly what is presented. Depending on what is of interest we have used either RPS or Matlab for the presentations of the results in this report. Below, the five integrated surface plot presentations are described. All the surface plots relate to the transmitter that acts as the best server.

## Coverage

The coverage, for example, is used to find out whether or not the signal power is strong enough for a specific radio receiver.

The coverage plot displays the largest received power from any of the transmitters. The power is calculated incoherently as:

$$P_{dB} = 10 \cdot \log_{10} \sum |a_i|^2$$

where  $a_i$  is the received complex amplitude of the i:th multipath component at the antenna terminal. An example is shown in Figure 3.1a).

## Best server

The best server plot shows which of the transmitters has the best coverage at each receiver position. This property is used, for example, when planning the positions of base stations in a stationary network. An example is shown in Figure 3.1c).

## Signal to Interference Ratio (SIR)

This ratio is used to determine the interference from other transmitters at the same frequency. This is used, for example, when planning the scheduling of frequencies in a stationary network. An example is shown in Figure 3.1d).

The signal to interference ratio plot shows the difference between the power of the best covering transmitter and the sum of the powers from all other active transmitters.

$$SIR = P_{dB \text{ best server}} - 10 \cdot \log_{10} \left( \sum 10^{P_{dB}/10} \right)$$

## Delay spread (Best server)

This quantity shows the amount of multipath components, which causes the enlargement of pulses in time. The delay spread is inversely proportional to the coherence bandwidth. An example is shown in Figure 3.1e).

The delay spread is the second order central moment of the power delay probability distribution function, and is calculated as follows:

$$\tau_{spread} = \sqrt{\frac{\sum \tau_i^2 P_i}{P} - \left( \frac{\sum \tau_i P_i}{P} \right)^2}$$

where  $P = \sum P_i$  and  $P_i = |a_i|^2$ .

This quantity gives an indication how well a radio designed for certain value of this parameter will work in the calculated environment.

## Angular spread

This property is used to determine the spatial diversity gain. The correlation between the antennas elements in an array is related to this value. It indicates the potential for using a MIMO-system (Multiple input antennas – multiple output antennas); if there is no angular spread there is no use of a MIMO-system. It is also useful when considering array beamforming. An example is shown in Figure 3.1f).

The angular spread is calculated for the azimuth angle,  $\varphi$ , at the receiver. It is the second order central moment of the angular power distribution. First the weighted mean value is calculated as:

$$\varphi_{mean} = \frac{\sum \varphi_i P_i}{P}$$

After this all the angles are re-arranged to be centred at the mean value:

$$\tilde{\varphi}_i - \varphi_{mean} \in [-180^\circ \quad 180^\circ]$$

Finally the angular spread is calculated using the re-arranged angles:

$$\varphi_{spread} = \sqrt{\frac{\sum \tilde{\varphi}_i^2 P_i}{P} - \left( \frac{\sum \tilde{\varphi}_i P_i}{P} \right)^2}$$

It is a bit dangerous to make the calculation in this way, since it is possible to get a wrong value on  $\varphi_{mean}$ . If the  $\varphi_i$ 's are all near  $-180$  and  $+180$  they may add up to for example, 0, when the average should be in the opposite direction. The results from the built in calculation differs a little bit from the plug-in version of the same, which might indicate that the built in version handles this problem.

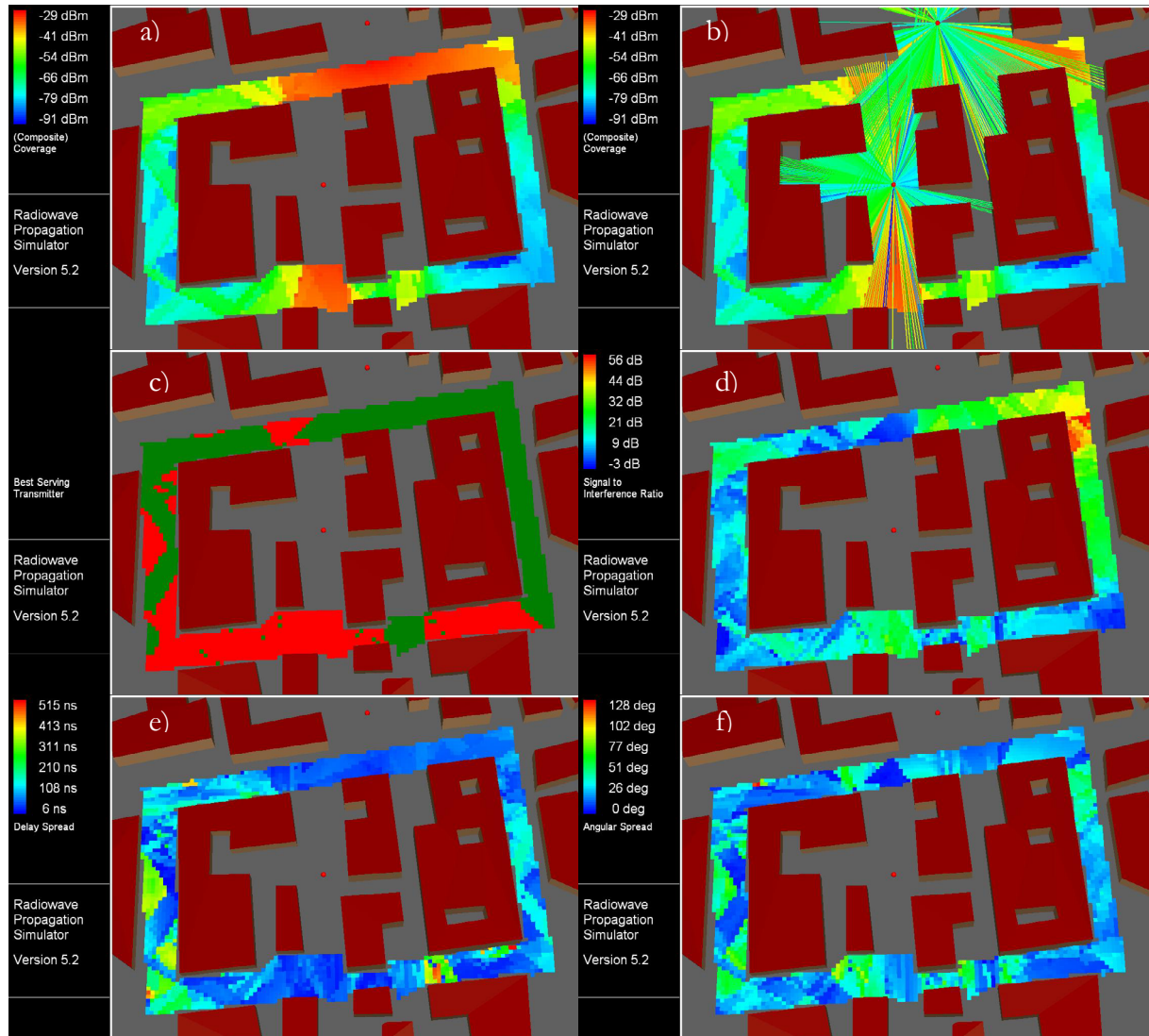


**Figure 3.1.** Examples of result plots for the static simulation, showing: a) Coverage, b) Coverage + first ray segment, c) Best serving transmitter, d) Signal to Interference Ratio, SIR, e) Delay Spread, f) Angular Spread.

### 3.3. Dynamic simulations

A dynamic scenario is when the transmitters and/or the receivers are moving. In RPS it is only possible to let the receiver move. The result from the static scenario is used as base for the dynamic simulation, in this the receiver can move with arbitrary speed through the environment. The movement is composed in the way described below. If movement of the transmitter is needed it is possible to make simulations with multiple transmitters very near each other but the simulation time will then be much higher.

Dynamic impulse responses can be generated for rather complicated receiver movements. Briefly these are constructed as follows:

- The starting point is the static channel data over a grid of receiver points which covers the entire area where movement will take place. An example of such an environment is shown in Figure 3.2.
- A number of circles with a given radius, so-called attractors, are placed in the geometry. These are marked as light blue circles in the environment; see Figure 3.2.
- The movement is composed of partial straight-line fixed-speed trajectories between attractors.
- The receiver moves between attractors from a random starting point within an attractor to a random break point within the next.
- The movement changes direction only within the attractor according to transition probabilities between the attractor and its neighbours.
- The total path thus formed is a so-called Markov chain.

One can only make use of the dynamic simulation results outside RPS. The result has to be exported either as ASCII files or as a Matlab readable file, which is described in section 3.4.

There are two Matlab functions distributed with the software which can be used for showing various results from the dynamic simulation. In Figure 3.3 the impulse response for one simulation is shown. In Figure 3.4 some other figures generated by the exported results are shown; at the left the route of the moving receiver, at the upper right the number of resolvable paths and at the lower right the id number of the active transmitting antenna for each step in the movement.

The resulting dynamic receiver signal is not interpolated. When the receiver is located anywhere within a grid cell it is given a constant signal equal to the calculated signal in the midpoint of the cell. Hence the time-variant impulse responses do not show any small scale fading; see Figure 3.5.

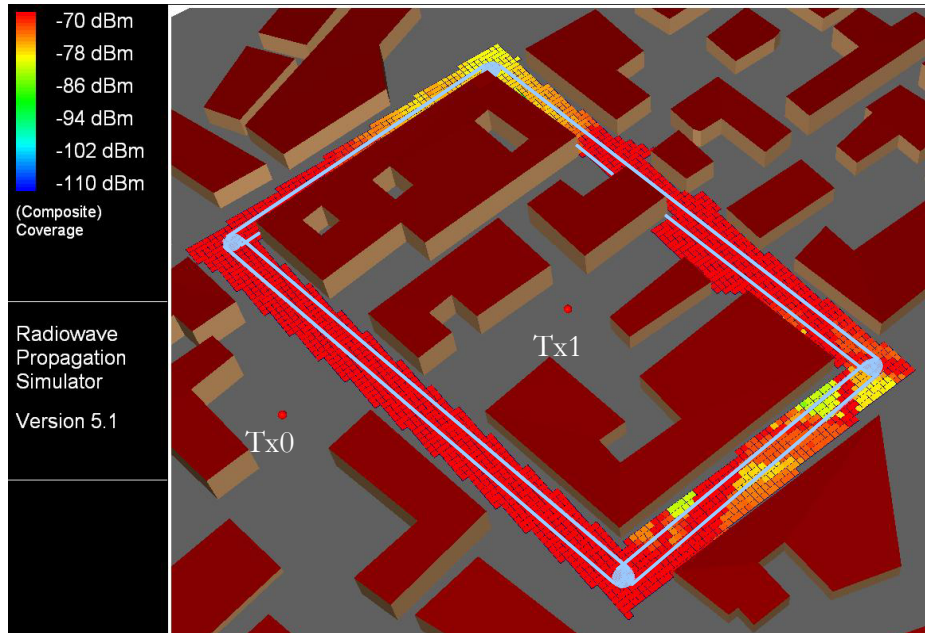


Figure 3.2. This figure shows the coverage over the predefined field of receivers used for the dynamic simulation. The light blue areas in the figure are the attraction areas and the thin lines between them are the boundaries within which the dynamic simulation can take place.

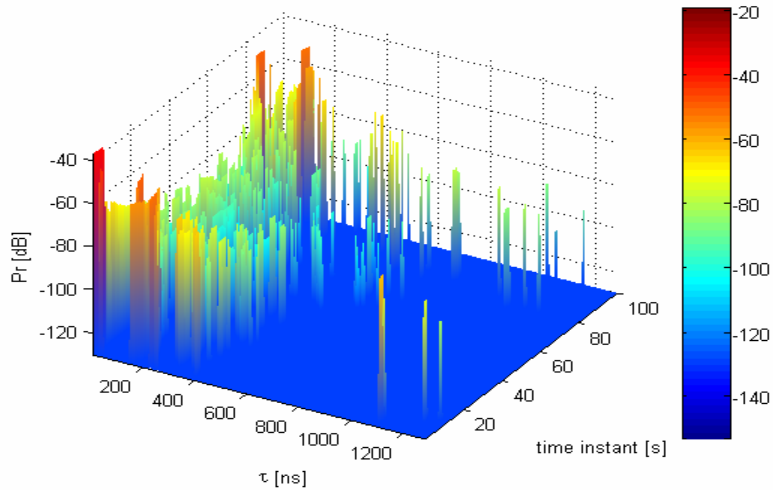


Figure 3.3. The impulse response for each of the steps in the dynamic simulation.

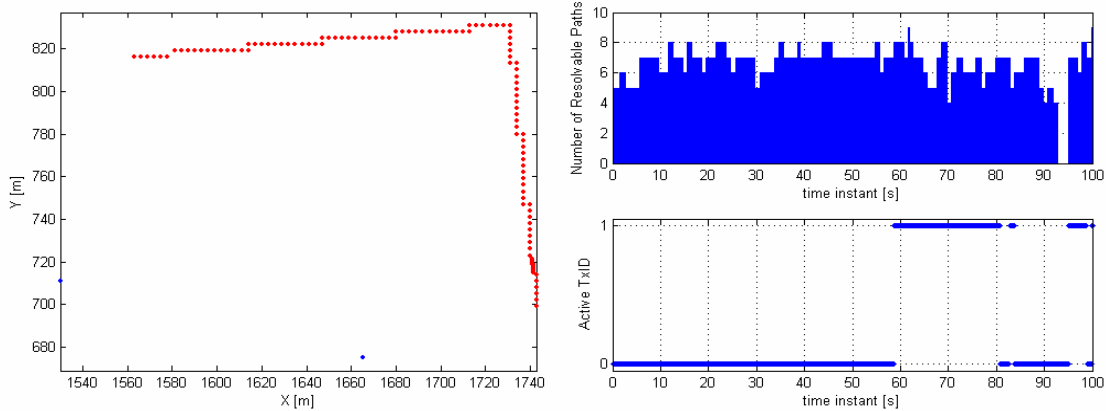


Figure 3.4. At the left, the route of the dynamic simulation is shown. In this case the starting point is in the upper left corner. The transmitters are marked with blue dots. At the upper right, the number of resolvable paths for each step in the dynamic simulation is shown. (The maximum for this simulation was set to 10.) The lower right shows the number of the active transmitter (0 or 1) for each of the steps in the dynamic simulation.

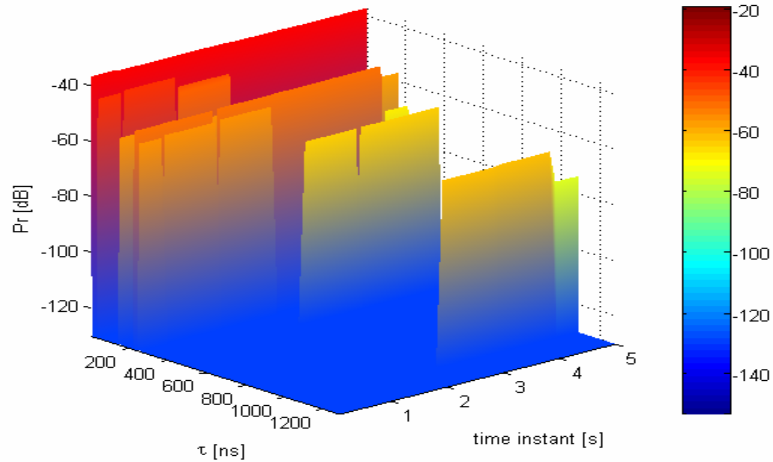


Figure 3.5. This figure shows first the section of the impulse response in Figure 3.3. In this dynamic simulation we have used a time interval small enough to retrieve more than one step in the region for one receiver. The receiver area is 3x3 metres, the time interval 0.1 s and the velocity is 3 m/s. From this figure one can see that the dynamic impulse response does not show any small scale fading.

### 3.4. Import/Export of data

In this section some of the import and export options are described.

#### Import object list

We start with the only import option we have used so far, which is the import object list. In an object list each row describes what material layer the building section belongs to, how many corners it has and at which points x, y, z in space these are positioned. In Figure 3.6, a simple building imported from the object list below is shown.

```

6 FILEVERSION
F GROUND DEMO 4 -10 -10 0 10 -10 0 10 10 0 -10 10 0
F ROOF BUILDING1 4 -5 -6 3 -5 6 3 0 6 7 0 -6 7
F ROOF BUILDING1 4 5 6 3 5 -6 3 0 -6 7 0 6 7
F WALLS BUILDING1 4 -5 -6 0 -5 6 0 -5 6 3 -5 -6 3
F WALLS BUILDING1 5 -5 6 0 5 6 0 5 6 3 0 6 7 -5 6 3
F WALLS BUILDING1 4 5 6 0 5 -6 0 5 -6 3 5 6 3
F WALLS BUILDING1 5 5 -6 0 -5 -6 0 -5 -6 3 0 -6 7 5 -6 3
C END

```

The properties for the material layers are set separately in RPS. Holes in buildings can be represented if first the outer line of a roof is described and then the inner line describing the hole, all on the same row in the object list.

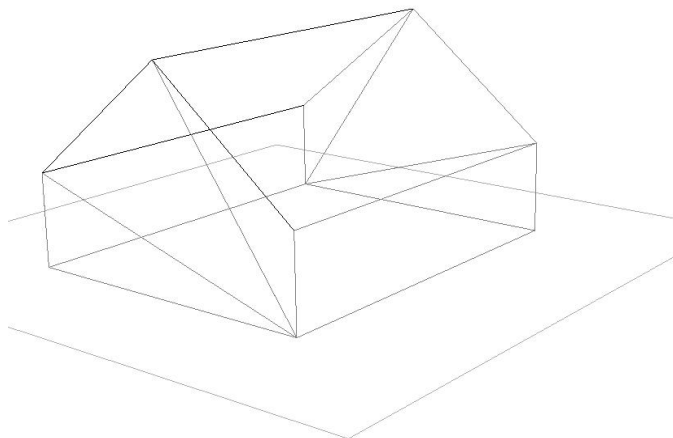


Figure 3.6. The building based on the object list shown above.

#### Save

The save command saves the simulation as it is when the command is executed. If the simulation is finished, its result will be saved. Otherwise the simulation environment and the transmitters and receivers and other settings which are used are saved. Alternatively, intermediate results during the simulation or results from a part of the simulation can be saved. However, it is not possible to use these results when starting a new simulation if they do not correspond to a transmitter which is fully calculated.

Irrespective of whether ray paths are stored or not, all information about the impulse responses at each receiver (spatial, temporal, and amplitude) is generally saved in the results.

## Result export

There are five export options available for the results from the static simulations and two for the dynamic:

- Export received power and delay spread
- Data as ASCII file
- Export DOA as ASCII file
- Export static data as ASCII-matrices in multiple files
- Export static data as matrices readable with Matlab
- Export dynamic data as ASCII-matrices in multiple files
- Export dynamic data as matrices readable with Matlab

The files using ASCII-format are easier to use when one wants to look directly at data to achieve a general view and if the output is not post-processed in Matlab. The data exported as ASCII exports all the multipath components, which means that the bandwidth is, in principle, infinite. Exceptions to this are when the ASCII formats with multiple file outputs or the Matlab format are used for the export; then the bandwidth used during the simulation is pre-selected for the export. It is, however, possible to change the bandwidth before the export is done.

The export options are further described in Appendix A.

## 3.5. Material properties

The material properties of the buildings are essential since they form the basis of how the waves propagate. The material properties affect the propagation through the medium and what is happening when the materials are changed; the reflection, diffraction and penetration depend on it. The parameters depend on the frequency, but the supplied database with material properties is only given for one frequency. One problem is that the dependence on the frequency is different depending on the materials and in general not known for the materials used. We will briefly discuss two different approaches how the recalculation can be done and our reason for using one of them.

The materials properties in RPS are described by the relative dielectric constant and the thickness of the material. Calculation properties are also assigned to the different types of material and one can decide if reflections, diffractions or penetration are to be allowed for the material. In our simulations we have used only three materials, one for the roofs, one for the walls and one for the ground. Another property that can be assigned to a material is to treat it as a Digital Elevation Model, DEM. This means that the ground can be set to be a DEM layer instead of a material layer. A consequence of this is that the height of transmitters and receivers can refer to this layer instead of the reference level,  $z=0$ , which usually is the mean sea level.

To minimize unnecessary calculations it is a good idea not to allow penetration through the ground. It is also a good idea not to allow diffraction for the ground layer.

In RPS the relative dielectric constant is given as  $\epsilon_r = \epsilon' - i\epsilon''$ . Next, we describe two different approaches to the frequency scaling of  $\epsilon''$  that give quite different results.

At the RPS website it is said that:

The materials database contains numerous entries for several frequencies published in the literature. Interesting publications are referenced below. The relation between  $\tan \delta$  and  $\epsilon$  is given by the following equation:  $\tan \delta = \frac{\epsilon''}{\epsilon'} = \frac{\sigma}{\omega \epsilon}$  with  $\epsilon = \epsilon_0 \epsilon'$ .

The real part of the dielectric constant (the permittivity) remains constant over a wide frequency range. The imaginary part can be determined for frequencies not listed here roughly by using the equation above with a constant conductivity  $\sigma$ .

Using constant conductivity  $\sigma$  has the consequence that  $\epsilon''$  depends on the frequency as:

$$\epsilon''_{\text{new}} = \frac{f_{\text{old}}}{f_{\text{new}}} \epsilon''_{\text{old}}$$

If we instead use the expression  $\epsilon_r = \frac{\epsilon_s + j\omega\tau\epsilon_\infty}{1 + j\omega\tau}$  from [Blomquist *et al.*, 1968], we get

$$\begin{aligned} \epsilon' &= \frac{\epsilon_s + (\omega\tau)^2 \epsilon_\infty}{1 + (\omega\tau)^2} \\ \epsilon'' &= \frac{\omega\tau(\epsilon_\infty - \epsilon_s)}{1 + (\omega\tau)^2} \end{aligned}$$

If we assume the form:  $\epsilon'' = \frac{\sigma}{\omega\epsilon_0}$ , then we get from the above formula:

$$\sigma = \frac{\epsilon_0 \omega^2 \tau (\epsilon_\infty - \epsilon_s)}{1 + (\omega\tau)^2}$$

This gives the following frequency scaling formula:

$$\epsilon''_{\text{new}} = \frac{f_{\text{new}}}{f_{\text{old}}} \epsilon''_{\text{old}}$$

Which is the opposite frequency dependency to the expression using constant conductivity. We have used the value  $\tau = 1,9 \cdot 10^{-11}$  for water.

We have used the latter expression when scaling the imaginary part for the material used, since we consider water to contribute most to the property of the material. In Table 3-1, the properties for the materials we used are shown. The highest frequency, 1.8 GHz, is the one taken from the materials database in RPS.

**Table 3-1. The recalculated material properties used in our simulations.**

Name	Material	$\epsilon'$	$\epsilon''$ at 50MHz	$\epsilon''$ at 250MHz	$\epsilon''$ at 400MHz	$\epsilon''$ at 920MHz	$\epsilon''$ at 1.8 GHz
DEM	Street (may be wet...)	15	1.9	9	15	35	70
ROOF	Concrete	3.5	0.025	0.125	0.2	0.46	0.9
WALLS	Reinforced concrete, outer wall	5	0.011	0.056	0.089	0.2	0.4

### 3.6. Ray launching

The concept of ray launching is quite easy to understand but it is quite hard to make a good implementation of it. The main idea is that rays are launched in all directions and when they hit an object they either reflect off, diffract over it or penetrate through the object, or arbitrary combination of these. Thereby the ray will possibly split and produce new rays which will hit a new object or maybe the receiver. This goes on until any of the stop conditions is reached. The one stop condition which is mandatory is the noise floor; rays with power less than the floor are cancelled.

In RPS the rays are accompanied by ray tubes; see Figure 3.7. The sphere which describes the wave front is divided into rectangular cones with sides corresponding to the step-size of azimuth,  $\Delta\varphi$ , and elevation,  $\Delta\vartheta$ ; see Figure 3.7. Ray splitting is used to split the ray cones when reaching a maximum area of the cross section, (the base of the cone); see Figure 3.7. The cones will only split when they hit an object and hence the splitting is not active if there is a long distance before the objects are reached. With such a scenario it is better to launch a denser grid of rays, with smaller steps in azimuth and/or elevation, to be certain that all diffraction edges are found. This was not known to us when we decided on the simulation settings used for the simulations in this report.

A fundamental property of ray launching is that one cannot guarantee that adjacent ray tubes join smoothly when the land in the receiver area. There may be some gaps between them, or they may overlap in some areas. Hence some receivers may lose a ray contribution they should have had; others may get a ray contribution too much.

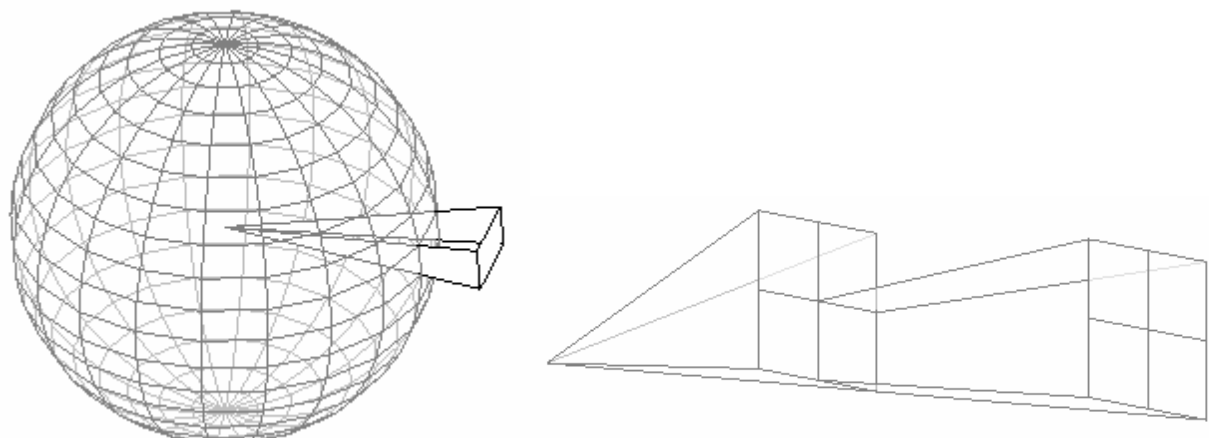


**Figure 3.7.** At the left the concept of dividing the sphere in ray tubes is shown ant at the right the concept of ray splitting.

When setting up the ray launching there are several parameters which have to be accounted for, see Figure 3.8.

First we will deal with the launching settings. These parameters define in which directions the rays are launched and their spacing, i.e. the step sizes in azimuth,  $\Delta\varphi$ , and elevation,  $\Delta\vartheta$ . The coordinate system used in RPS is North to East oriented; see Figure 3.9.

There are some cancellation settings which should be used for the simulation. As mentioned above, the noise floor is the lowest power a ray can have before the tracing for that particular ray will be cancelled. It is important to choose this parameter carefully, if it chosen badly either the simulation will take much longer time than necessary or too few or maybe no rays at all will reach the receiver.

One can decide whether reflections, penetrations and diffractions should be allowed or not, and a limitation on the maximum number of each of those processes before ray cancellation can also be chosen.

We have never allowed penetration for our simulations since this would give very long simulation times. Also the material properties and wall thickness are not known well enough.

Some simulations were made without any limitations and then the maximum number of diffractions never attained a value higher than 5. Because of this we have usually not allowed more than 6 diffractions. During the simulation it is possible that higher values are reached before the simulation is cancelled for some other reason, and thus we have put a limitation on this value to prevent unnecessary calculations.

The restriction on maximum delay cancels unnecessarily long rays, e.g. those that are launched into empty space.

The save ray path option determines whether the whole path of each ray reaching the receivers should be stored or not. If it is stored, it can be shown in the RPS environment together with the buildings. For big simulation scenarios, the simulation is slowed down if the ray paths are saved. In any case, the first and last ray segment will always be saved not to lose any necessary information.

We have made some tests with different settings of spacings of the ray cones and ray splittings; the results of these are shown in section 3.9. In that section we also present a test of the concept of receiver or receiver area and a discussion on that.

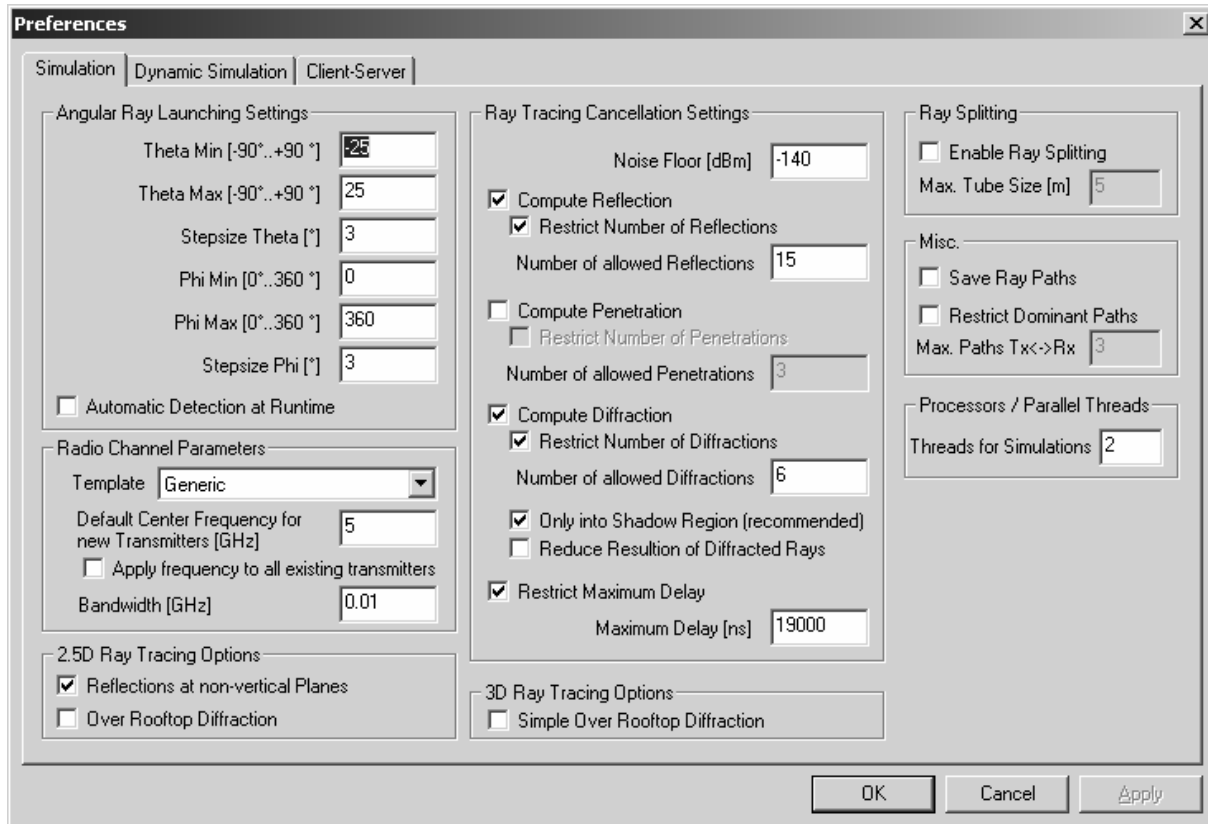


Figure 3.8. The general preferences window includes all settings which affects the simulation setup. (This setting was used for the simulation case narrowband 394 MHz.)

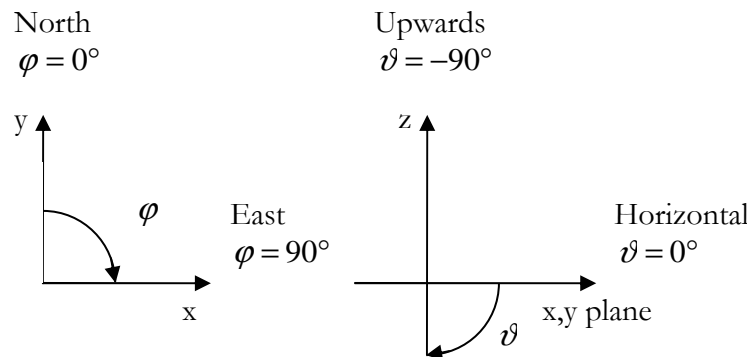


Figure 3.9. The coordinate system used in RPS.

### 3.7. Empirical model

As an alternative to ray tracing the package contains an empirical calculation using the Walish-Ikegami model. This can also be executed as a so-called hybrid option after the deterministic ray tracing has been done. This has the effect that receiver positions not reached by any ray will be given an empirical signal strength. In this way one can always obtain a complete coverage map. So far, we have not tested this hybrid option in our calculations.

### 3.8. Antennas

There are several antennas included with the program, most of them for quite high frequencies. Each antenna is based on the vertical and horizontal antenna patterns which are interpolated to a three-dimensional antenna pattern in the calculations.

The antennas, except for isotopic source, are imported into the scenario, and afterwards assigned separately to the receivers and transmitters.

It is quite easy to implement other antennas if the vertical and horizontal antenna patterns are known. One just has to remember to use the coordinate system of RPS (see Figure 3.9) and also that the description of the antenna patterns should be in attenuation described in dB, which is gain with the opposite sign.

The gain value and a polarisation can be specified for the antenna. The polarisations possible to use are ‘linear vertical’, ‘linear horizontal’, ‘right hand circular’ and ‘left hand circular’.

An antenna is described by 3 data files. One is the header file of \*.cfg format, which contains the antennas: ID, total gain [dB], and the two file names for the respective horizontal and vertical antenna diagrams. The extension for these are \*.dat. There are two formats supported for the antenna diagrams:

Format 1: angle [tab] attenuation [tab] optional phase

Format 2: angle = attenuation, phase

Below an example of the files is shown.

```
##///////////////////////////////
## This file is created by the Matlab function yagi2RPS
##///////////////////////////////
ID = FOAyagiRx445
Gain = 13.9776
HorizontalDiagram = FOAyagiRx445hh.dat
VerticalDiagram = FOAyagiRx445vv.dat
```

```
#Angle = Attenuation [dB] , Phase
.000 = 0.000000 , 0.00
1.00 = 0.001521 , 0.00
2.00 = 0.018381 , 0.00
3.00 = 0.052193 , 0.00
4.00 = 0.098709 , 0.00
5.00 = 0.148766 , 0.00
6.00 = 0.231926 , 0.00
7.00 = 0.315086 , 0.00
8.00 = 0.398246 , 0.00
9.00 = 0.512672 , 0.00
10.00 = 0.628042 , 0.00
```

## Antenna interpolation

In deterministic channel propagation calculations the antenna gain is in general required in all spatial directions. What is at hand are usually only the horizontal and vertical antenna diagrams, from measurements or from antenna theory. Then some method of interpolation from these antenna diagrams to the antenna function for arbitrary ray directions is needed. The technique implemented in RPS is described in section 10.7 of the RPS manual. According to this the gain  $G$  (dB) in azimuth  $\varphi$  and elevation  $\vartheta$  (degrees) is given by:

$$G(\varphi, \vartheta) = G(0^\circ, 0^\circ) - \{C_\varphi(\varphi) + (C_\vartheta(\vartheta) - C_\varphi(0^\circ))D + (C_\vartheta(180^\circ - \vartheta) - C_\varphi(180^\circ))(1 - D)\}$$

$$D = |180^\circ - \varphi|/180^\circ$$

$C_\varphi(\varphi)$ : relative magnitude of *attenuation* (dB,  $0^\circ$  to  $360^\circ$ , horizontal diagram)

$C_\vartheta(\vartheta)$ : relative magnitude of *attenuation* (dB,  $-90^\circ$  to  $90^\circ$ , vertical diagram)

Adding the horizontal and vertical gains is here equivalent to multiplying the field strengths from the horizontal and vertical contributions. The quantity  $D$  is a weighting factor which emphasizes different parts of the vertical antenna diagram in the half spaces in the forward and backward directions. Actually, the vertical diagram will be needed in the entire interval  $-90^\circ$  to  $+270^\circ$ . Note that the attenuations are given positive values for negative relative gains.

An alternative approach to this kind of interpolation has been described in [Lundborg and Ladell, 2003]. It was devised especially for yagi-like antennas and uses a somewhat more complicated trigonometric weighting between the horizontal and vertical diagrams. That paper also describes the transformation of the antenna function for arbitrary orientation of the antenna.

To illustrate the two approaches, we consider the particular example of a seven element vertical yagi antenna. In this case the field from the antenna will have only a vertical ( $\vartheta$ -oriented) component. The “exact” antenna function has been calculated in the numerical electromagnetic code NEC and is given in Figure 3.10. The interpolated antenna function from the method of [Lundborg and Ladell, 2003] is shown in the next figure, Figure 3.11. The interpolated result is almost indistinguishable from the exact result. However, we point out that this technique has only been tested for yagi antennas.

The corresponding RPS interpolation described above is shown in Figure 3.12. The main and back lobes of the antenna are represented fairly accurately, but other directions show poor agreement with Figure 3.10.

If we wish to model yagi antennas in RPS, we should consider implementing the more accurate antenna interpolation scheme.

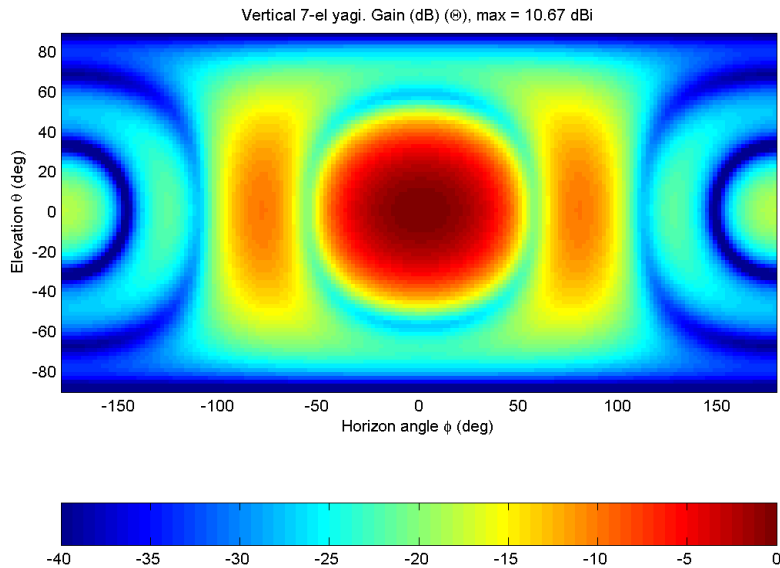


Figure 3.10. Antenna function for vertical 7 element yagi calculated in NEC.

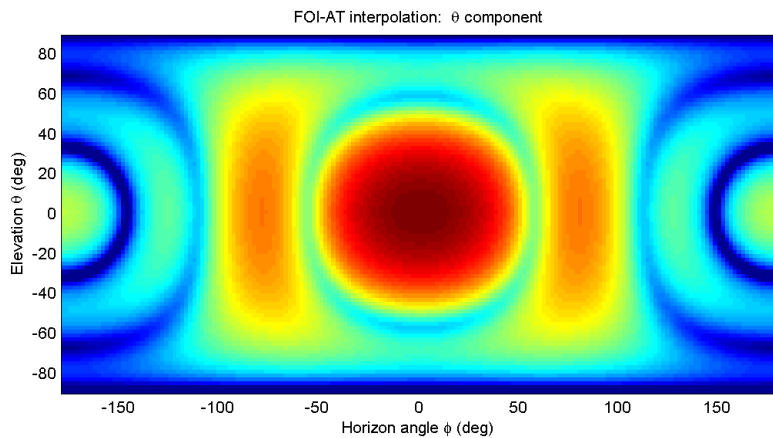


Figure 3.11. Interpolation from the horizontal and vertical diagrams for the same antenna using the technique of [Lundborg and Ladell, 2003].

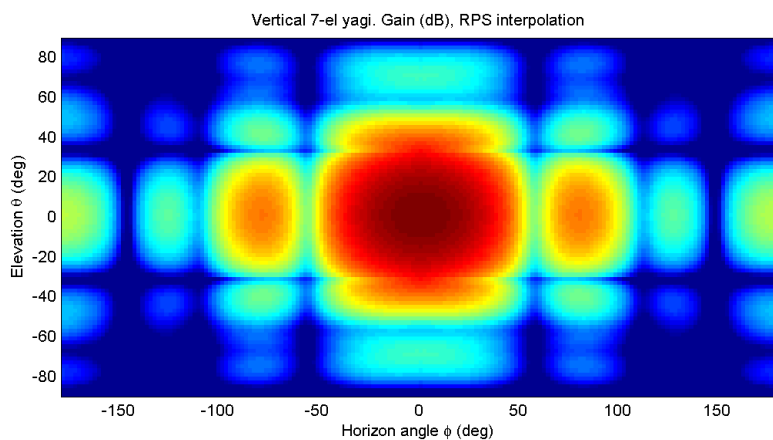
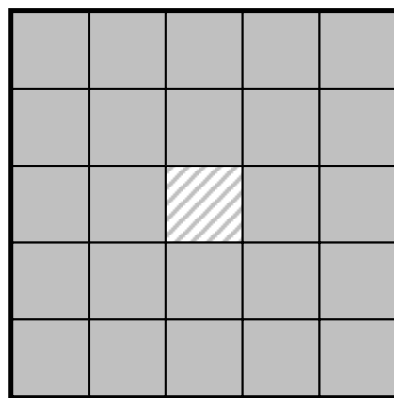


Figure 3.12. Interpolation from the horizontal and vertical diagrams for the same antenna using the technique of RPS [RPS user manual v. 5.2, 2004].

### 3.9. Experiences of RPS and tests

#### Test of received rays

We have made some tests to find out which rays contribute to the field strength for a receiver position. To this end we performed a test with two sets of receivers. In the first set we had one single receiver area of size  $10 \times 10$  meters, in the other set we had 25 receivers of size  $2 \times 2$  meters each. Both sets were placed with the same origin, see Figure 3.13.



**Figure 3.13. Both sets of receivers. The black square is the  $10 \times 10$  m receiver and the grey squares are the set of  $2 \times 2$  m receivers. The striped square in the centre is of particular interest.**

The figures below show the result for the different sets.

When we examined the exported results we found that the rays that contribute to the  $10 \times 10$  m receiver and to the centre  $2 \times 2$  m receiver are exactly the same; as can be seen in Figure 3.14 and Figure 3.15. In the latter figure the signal reduction with increasing angle of diffracted rays can also be seen.

The results from the test give that the concept of receiver area actually is a bit misleading. The receiver is effectively not an area but the mid point of the area. The rays contributing to one receiver are the ones whose ray tubes cover the mid point.

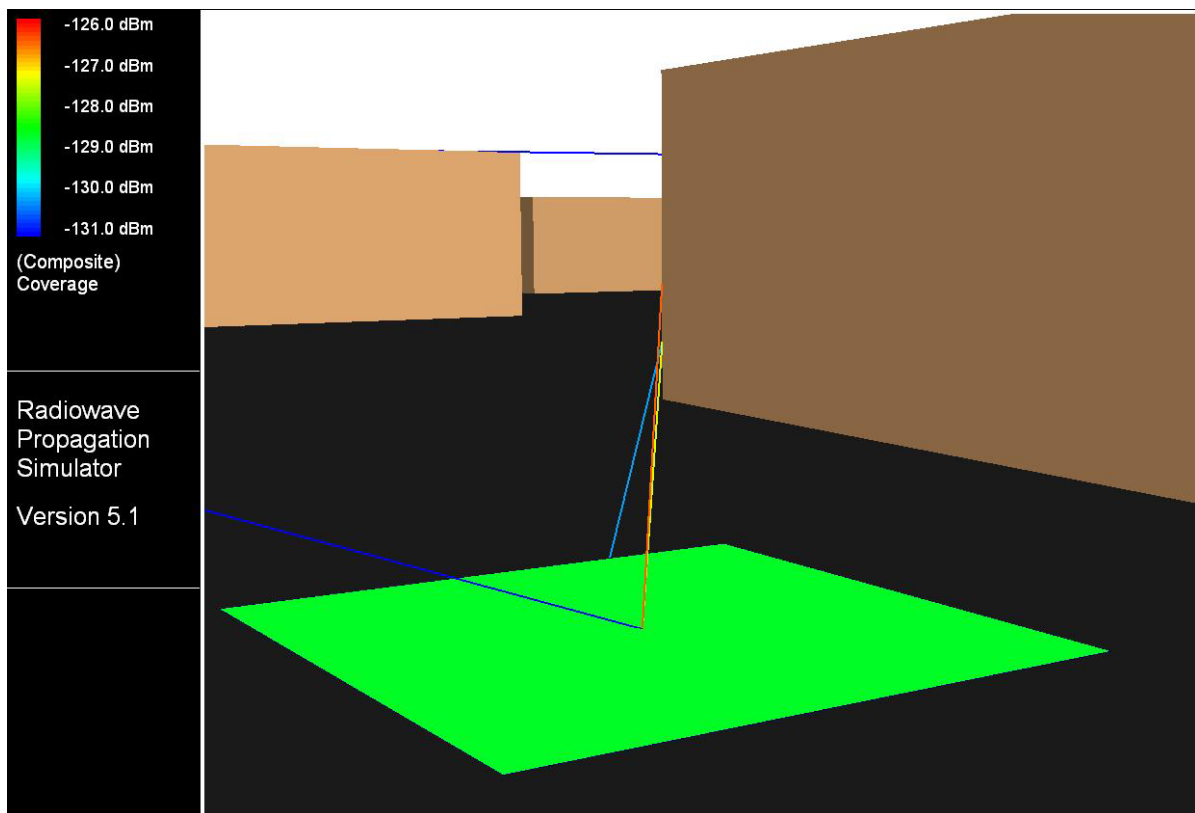


Figure 3.14. The received rays at the receiver sized 10×10 metres. 4 rays contribute to the field.

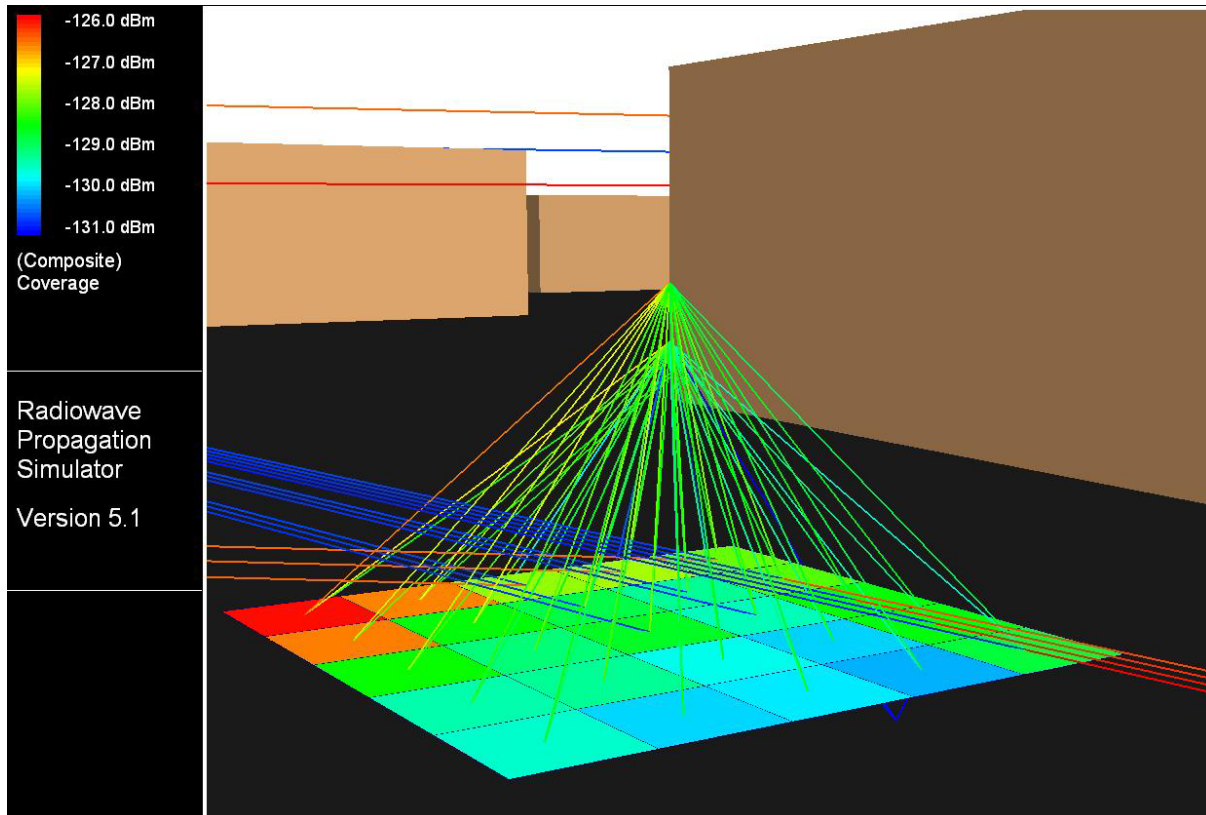


Figure 3.15. This shows the resulting field at the field of receivers sized 2×2 metres. One can see that the colour of the square in the centre is the same as in the figure above. One can also see that the magnitude of the diffracted rays decreases with increasing diffraction angle.

## RPS ray launching

Early in the work with the software we did some systematic tests where the ray launching settings were changed using RPS 5.1. The tests were made to improve our understanding of the 3D ray launching algorithm. In the manual [RPS 5.1] there is only a brief description on the ray launching approach and nothing said about the specific algorithm. Our first view on ray launching was as follows:

- When the receiver area is increased, a larger number of rays will fall within it.
- When a denser grid of rays is launched, a larger number of them will fall within the receiver area.

Based on our previous knowledge the results we got were to us quite counter-intuitive. The explanation for this can be found by carefully reading the text on ray tubes in the RPS user manual, sec 3.4.5, p 72: *"If a receiver is located within a ray tube, the complex E field ... are stored at this receiver."* Hence it is the opposite view from what we were thinking.

It is not a ray landing within a receiver *area*, but a receiver *point* being covered by a ray tube. This point of view was later on confirmed first by the test described earlier, and later by the software developers.

With this change of view we believe everything falls into place:

- When the ray tube is large it has a greater chance to cover a receiver point.
- Ray splitting increases the number of rays dramatically, but each tube has a smaller chance to cover a receiver.
- Ray splitting does not take place in space – only if the splitting condition is fulfilled when the ray hits a surface.
- The limiting case with infinitely thin ray tubes should give the most correct representation; hence one should do the calculation with a sufficiently large number of rays. How big is this number?
- If the ray tube cross section is allowed to go to zero the number of rays contributing to a receiver point should approach a constant value.
- A large ray tube will cover *everything* after diverging through a number of reflections; hence the very large number of detected rays we get for the 3 by 3 degrees case below.
- The number of launched rays + the number of ray splittings might be a relevant parameter to judge the resolution of a calculation.

The user's manual recommends an angular grid in the range of 0.5° to 5° depending on the scenario [sec 5.2.3.1, p 135]. One important piece of information regarding this choice is that the algorithms will not identify a diffraction edge at a roof unless there is a ray that actually hits the roof. With our type of scenarios with rather long distances in free air before the ray reaches the surroundings of the receiver this means that a very dense grid of rays must be launched in order for a roof to be hit. Note that it is the projected cross section of the roof as seen from the ray direction that is of importance here. This is not well documented in the manual and the information reached too late to affect the simulations we have done so far.

With too sparse a grid of rays too few rays reach into shadow zones, resulting in too pessimistic calculation of coverage. Another option which might amend this and also saves execution time is the simple over rooftop calculation. It considers the height profile of the buildings in the vertical

cross-section between the terminals and performs a UTD calculation with the break points of the profile. When this option is chosen the ordinary diffraction algorithm will only consider diffractions at *vertical* edges. However, we did not use this, as its function was not clear from the manual.

Regarding received signal, the manual talks about *wideband signal power*, meaning addition of individual ray powers (i.e. what should properly be denoted incoherent addition) – versus *narrowband signal power*, probably meaning addition of complex field strengths (this is called incoherent addition in the manual, but it is rather coherent addition) [sec 6.6.1, p 176].

We did some tests where we varied the step size in elevation and azimuth and used different values for the ray splitting as shown in table 3-2. We did these simulations using RPS version 5.1 which uses a different condition for the ray splitting than mentioned in section 3.6. In version 5.1 it is the mean length of a ray cone, which is given instead of the maximum side length of the bottom of the cone.

In the frames of figure 3.16 we have sorted the results in the order of the sum of launched rays and the number of ray splittings.

In the topmost frame the sum of the complex signal contributions at each of the 57 receivers is shown (coherent addition). A slightly different way of presenting the result is seen in the frame in the centre, where the sum of the signal powers is shown (incoherent addition). In the bottom frame the receivers which detected a signal are indicated for the respective simulation setting. In this figure the total number of launched and split rays (Trans. rays + No. of splitting in Table 3-2) are highest at the top (red) and lowest at the bottom (yellow). Looking in this figure one can see that the different settings give contributions to different receivers. In this test the total number of transmitted rays and ray splittings seems to be at least somewhat correlated with the number of receivers reached. The number of detected rays seen in the Table 3-2 is not particularly correlated to the number of receivers reached or the total signal strength. What also can be seen is that in our test environment the spacing in azimuth and elevation of  $3^\circ$  seems to be a good choice for getting a high number of detected rays. The high number of received rays is caused by the diffraction over the last edge in the path giving contributions to many of the receivers, an example of this type of splitting of the rays can be seen in figure 3.15. The rays are split into new directions that lie on the diffraction cones; note that this is another effect than the ray splitting set by the user.

**Table 3-2. The simulation setting used and some statistics for the result.**

Filename	$\phi$ [ $^\circ$ ]	$\vartheta$ [ $^\circ$ ]	Ray split [m]	Trans. rays	Sim. time	Detected rays	No. of splitting	Reflections (mean/max)	Diffractions (mean/max)
az0.5el0.5grid5nosplit	0.5	0.5	No	83039	15'13"	168	0	4.59 / 7	1.33 / 3
az3el3grid5split70	3	3	70	2381	3'50"	124	54281	4.08 / 9	1.53 / 3
az3el3grid5split100	3	3	100	2381	2'08"	105	35191	3.6 / 9	1.7 / 3
az1el1grid5nosplit	1	1	No	20889	4'17"	90	0	3.4 / 6	1.92 / 3
az3el3grid5split200	3	3	200	2381	1'14"	447	17301	3.02 / 8	1.86 / 3
az3el3grid5split250	3	3	250	2381	1'14"	412	13170	2.83 / 6	1.95 / 3
az3el3grid5split300	3	3	300	2381	1'11"	456	9744	2.88 / 6	1.88 / 3
az1.5el1.5grid5nosplit	1.5	1.5	No	9347	2'23"	70	0	3.2 / 5	2.17 / 3
az2el2grid5nosplit	2	2	No	5283	1'54"	41	0	4.27 / 8	1.93 / 2
az3el3grid5nosplit	3	3	No	2381	1'21"	559	0	3.35 / 7	1.81 / 3

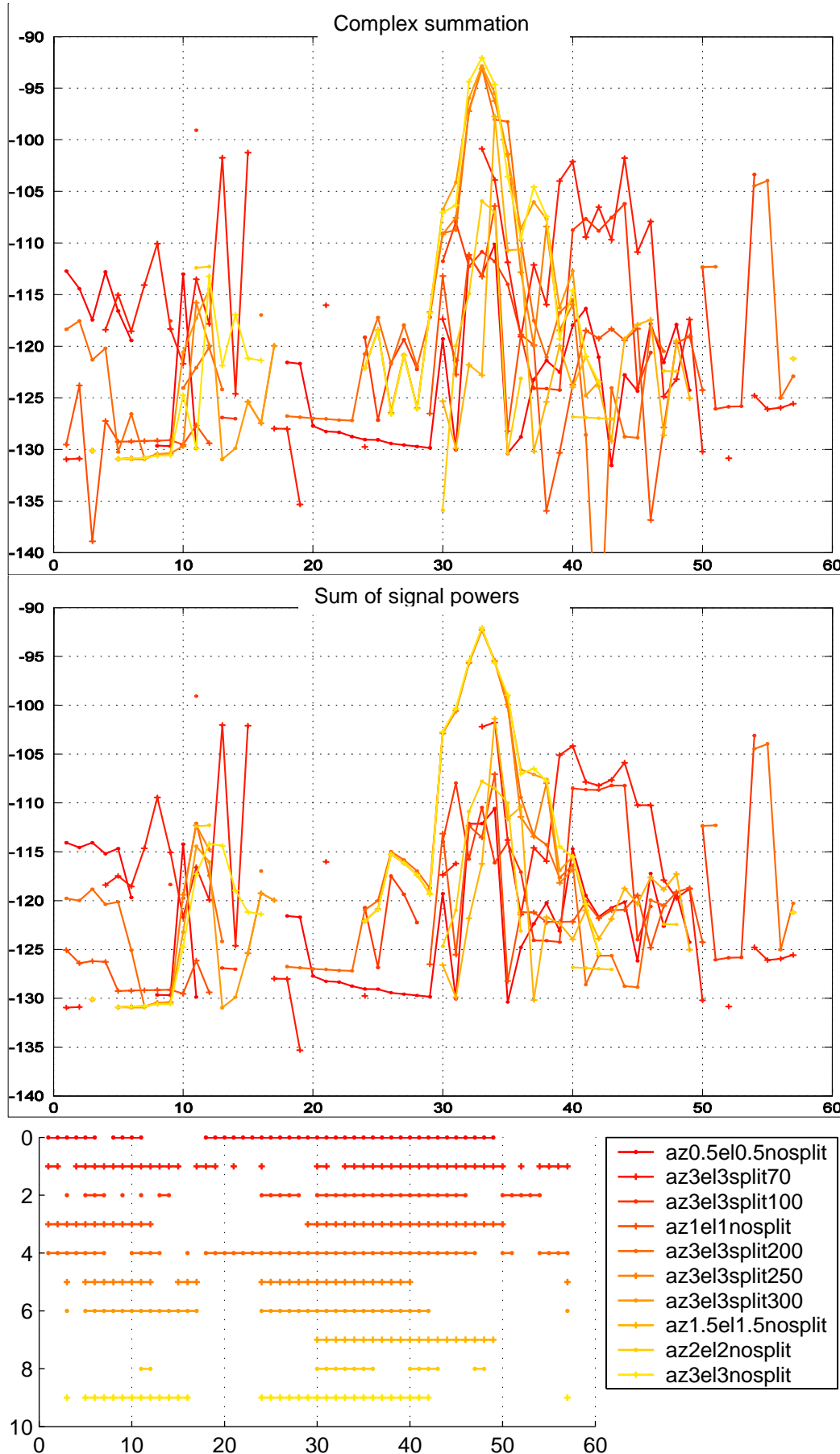


Figure 3.16. Tests of different ray launching settings

# Chapter 4 Comparison RPS vs. Stockholm measurements

To evaluate the feasibility of RPS we have compared the simulations with data from two propagation measurement campaigns in the Stockholm area. The first one is wideband measurement performed in the late 1970s. The second campaign is narrowband measurements performed in 2002.

To get reasonable simulation times we have put some restrictions on RPS concerning the size of the calculated area, maximum delay etc.

## 4.1. Wideband measurements

In the late 1970s a number of wide-band measurement campaigns were performed by FOA, in rural areas as well as in central Stockholm. The purpose was to determine the multipath characteristics of the radio channel. This was motivated by the gradual shift from analogue to digital radio equipment in military communications.

The measurement system consisted of a pseudo-noise modulated transmitter and a sliding correlation receiver [Cox, 1972]. The quadrature components of the complex impulse responses were stored on tape for off-line processing. For monitoring purposes the magnitude of the complex impulse responses were computed by an analogue device and shown on an on-line display [Stenström *et al.*, 2001].

Unfortunately, the raw data from these measurements are no longer available. What remains today are photos of power-delay profiles, either from post processed data or the on-line display, meant to be used for documentation purposes. Thus, the phase information of the measurements is lost.

We intended to use some of the measurements from Stockholm for comparison with simulations in RPS.

### 4.1.1 Measurement setup

The distance between the transmitter and the receiver is in the range of 2.9 to 3.4 km. The mobile transmitter antenna was placed at 2.6 m height on a car. The measurements were made while the car was driving through the loop marked blue in Figure 4.1. The receiver antenna was placed on the roof of what was then the FOA building, to the right of the area shown in figure 4.1. The height above ground was 23.1 m. Both antennas were omni-directional in the horizontal plane and vertically polarized. The frequency used was 445 MHz and the transmitted power was 60 W.



**Figure 4.1. The measurement route is marked blue and the particular section we have studied is marked green.**

After investigations of the photos of the power-delay profiles for the different measurement sections we decided to use the section marked green in Figure 4.1. This section has several distinct multi-path components within a limited delay range. This was important since the available data-set of buildings for Stockholm restricted the simulated excess delays to 5  $\mu\text{s}$ . From the photos we have extracted the impulse responses by means of a program called Irbilder, made by Lars Ladell at AerotechTelub [Stenström *et al.*, 2001].

A power delay profile shows the magnitude of the received power plotted against the delay. In the Figure 4.2 one can see that there are at least two distinct multipath components having a very short delay. In most of the measurements there is also a multipath component arriving after approximately 6  $\mu\text{s}$ , which corresponds to an excess distance of 1800m beyond the line-of-sight path.

### 4.1.2 Simulations

We have made several attempts to simulate this scenario but none of the simulations which were finished had enough rays reaching the receiver area. To increase the number of rays the noise floor was lowered, which gave much longer simulation times. However, these simulations could not be finished, so no results are presented here.

With recently obtained information concerning the operation of RPS this case can probably be calculated rather straightforwardly, but this could not be done before the printing of this report.

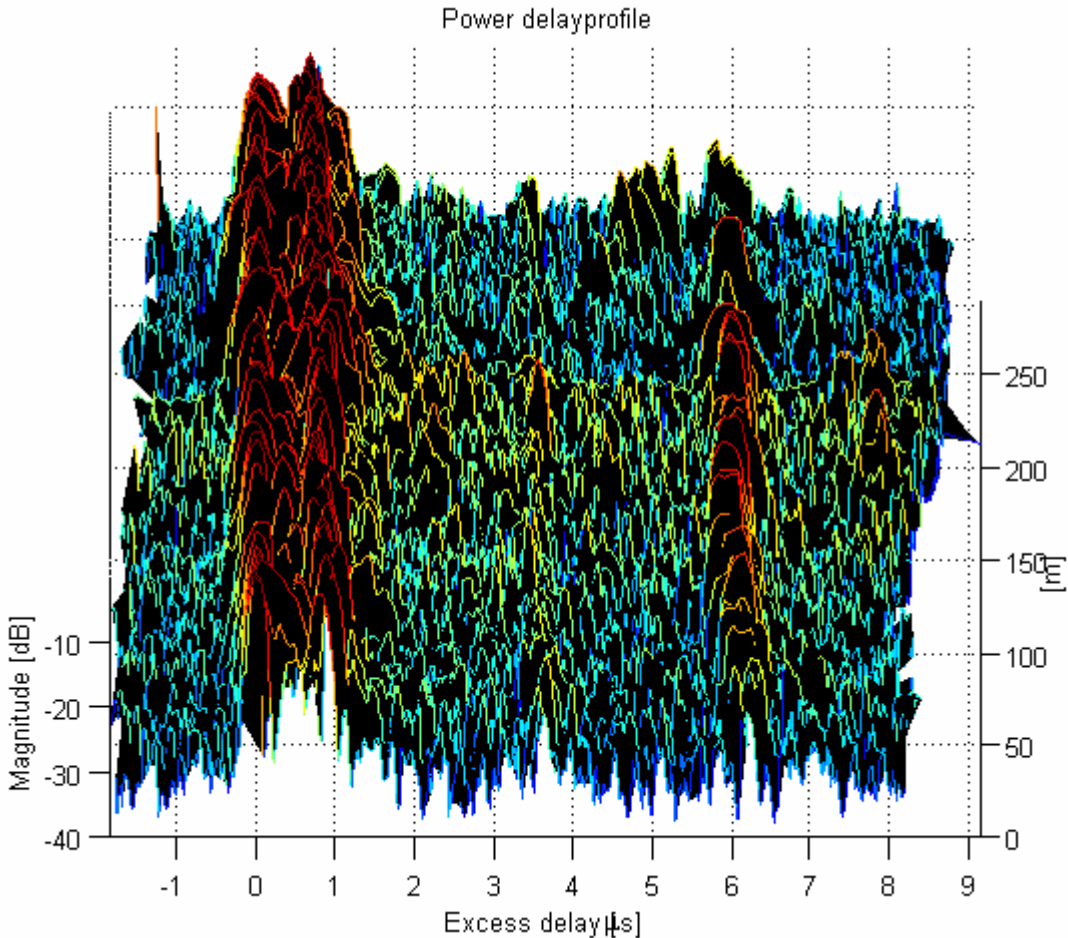


Figure 4.2. Measured power delay profile along the section marked green in Figure 4.1.

## 4.2. Narrowband measurements

In 2002 a new measurement series was performed with the receiver in the same area of Stockholm as was used for the transmitter in the measurements described in the previous section. Several transmitter sites were used. The measurements were done within a project named 3D, which was a joint project with participants from FOI, Linköping and AerotechTelub, Linköping and financed from the Swedish Defence Materiel Administration, FMV. The measurements were made by AerotechTelub, Arboga. The measurement setup is described further in [Gustafsson, 2002]; the results can be found in [Gustafsson and Ladell, 2002]; summarizing plots of the results is found in [Holm and Ladell, 2004].

These measurements are all narrowband; it was simply the signal strength of the unmodulated carrier that was recorded. The purpose for these measurements was for verification and validation of propagation models and programs such as RPS.

In these measurements two different routes for the mobile receiver were used. The inner of these routes was the same as for the old FOA measurements. The measurements were performed in five frequency bands at two frequencies in each band separated approximately 5 MHz, see Table 4-1. Seven transmitter positions were used, but in this report we will only use one transmitter site

at KTH, the Royal Institute of Technology. The resulting figures from all frequencies used for our simulations of this scenario are found in Appendix B.

The transmitter site at KTH is elevated compared with the receiver sites, see Figure 4.3. The distance between transmitter and the nearest receiver position is about 1 km and the overall extension of the receiving area is about 500×200 metres.

**Table 4-1. The frequencies used in the measurements.**

51 MHz	56 MHz
250 MHz	255 MHz
394 MHz	398.8 MHz
915.5 MHz	920.5 MHz
1794 MHz	1799 MHz

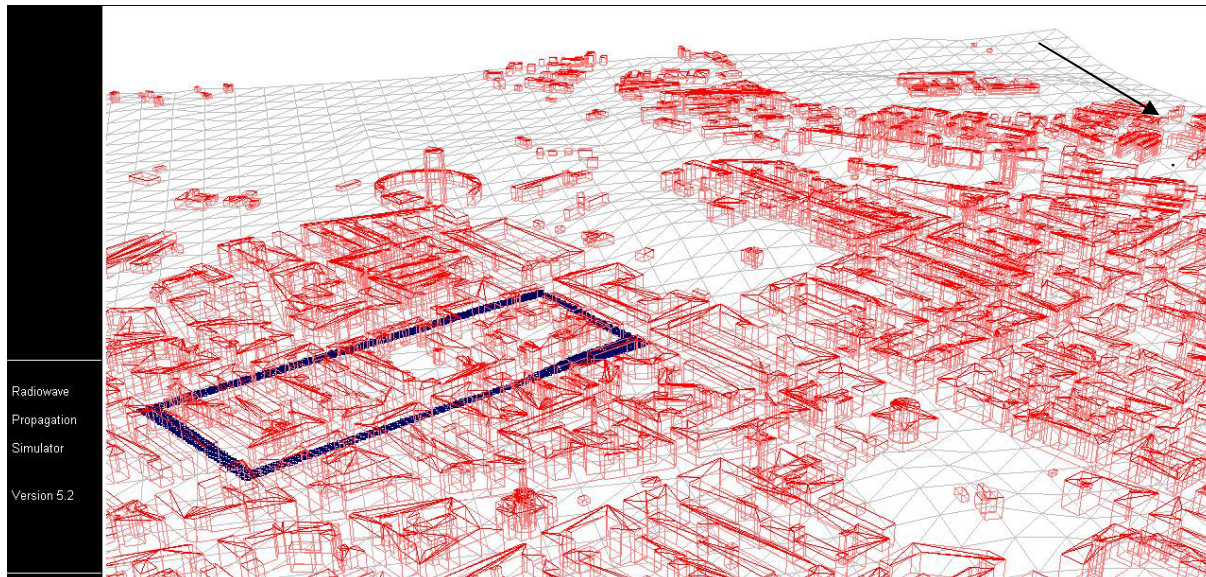


**Figure 4.3. A 3D wire-frame presentation of the buildings between the receiver sites, the blue rectangle, and the transmitter at KTH, the blue dot at the arrow.**

#### 4.2.1 Simulation Setup

For the simulation we used the 3D ray-tracing model in RPS. We chose to use the lower frequency in each pair of frequencies, see Table 4-2. The power at the transmitter was set to the same value as was used in the measurements, adjusted for cable loss, compression and antenna gain. At both transmitter and receivers we used isotropic antennas at a height of 2 m over the ground. The sensitivity of the receivers was adjusted for each frequency to achieve fairly the same number of received rays (differs quite a lot). If too high sensitivity is used at the receivers very long simulation times are obtained. The number of diffractions was restricted to 6 and the number of reflections was restricted to 15. We did not allow penetration at all, since these would give much longer simulation times. The step-sizes in elevation,  $\Delta\vartheta$ , and azimuth,  $\Delta\varphi$ , were set to  $3^\circ$  and the maximum delay for a path was set to 19  $\mu\text{s}$ , which corresponds to approximately 3 times the longest distance between transmitter and receiver.

The simulations were performed with RPS 5.2 with the rpe.dll dated 2004-08-24.

**Table 4-2.** The frequencies, transmitted power, noise floor used for the simulations at the different frequencies, together with the number of received rays and the simulation time. The simulations were parallelized using different number of computers.

Simulation frequency	EIRP dBm	Noise floor	Received rays	Simulation time [minute]
51 MHz	38.6	-95	120,626	775
250 MHz	36.6	-125	86,727	571
394 MHz	43.7	-140	199,659	2,340
915.5 MHz	38.5	-145	58,751	334
1794 MHz	38.6	-160	74,213	327

## 4.2.2 Comparison

We have made ray tracing simulations with the setup described above and also calculation using the simpler Walfisch-Ikegami (WI) model for comparisons with the measurements. The results for the simulations and the measurements are presented in full in Appendix B, as well as a discussion of the results.

When comparing the measurements and the simulations, we found the best agreement for the highest frequencies. This is also the range for which RPS was designed. In the ray tracing simulation at 394 MHz, Figure 4.5, some of the receivers have powers in the same range as the corresponding ones in the measurement, Figure 4.4. But most of the receivers have much lower powers, by approximately 15 dB. Apart from the level, the fading patterns from the simulations show a fair similarity to the measurements. For all 3D ray tracing simulations, made for the comparison with the measurements, the signal power is underestimated. Also, the WI-simulation at 394 MHz, Figure 4.6, gives a fairly good agreement with the measurement. In contrast to the ray tracing simulations, the WI-simulation overestimates the signal power for the low frequencies.

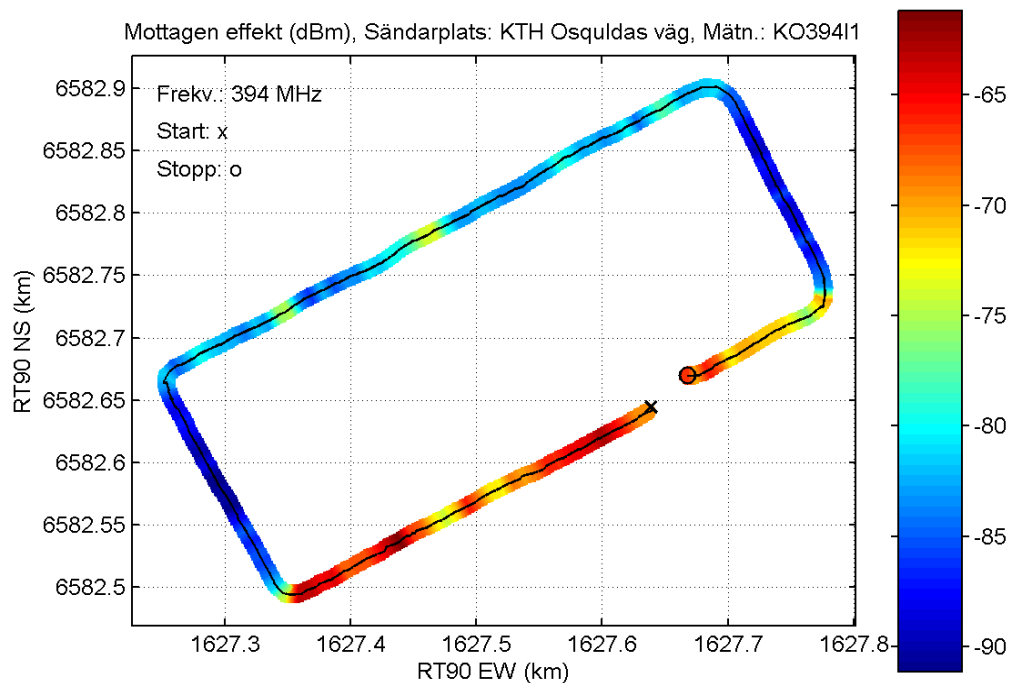


Figure 4.4. The results for the 394 MHz measurement.

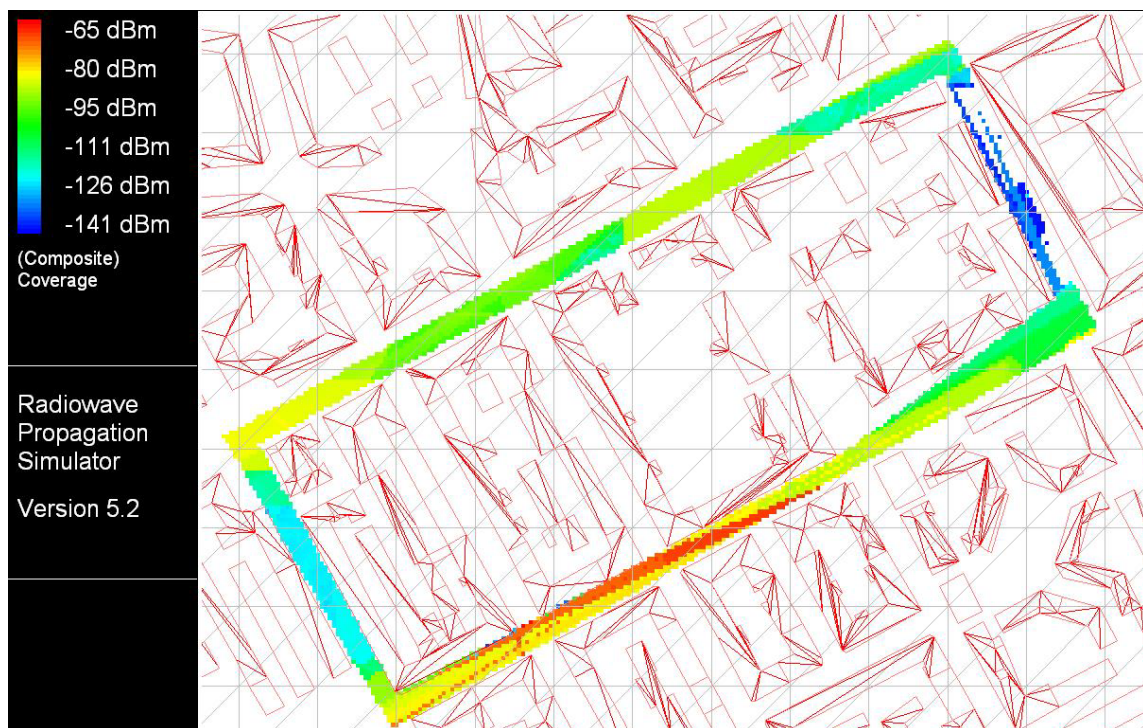


Figure 4.5. Result for the 394 MHz 3D-ray tracing simulation.

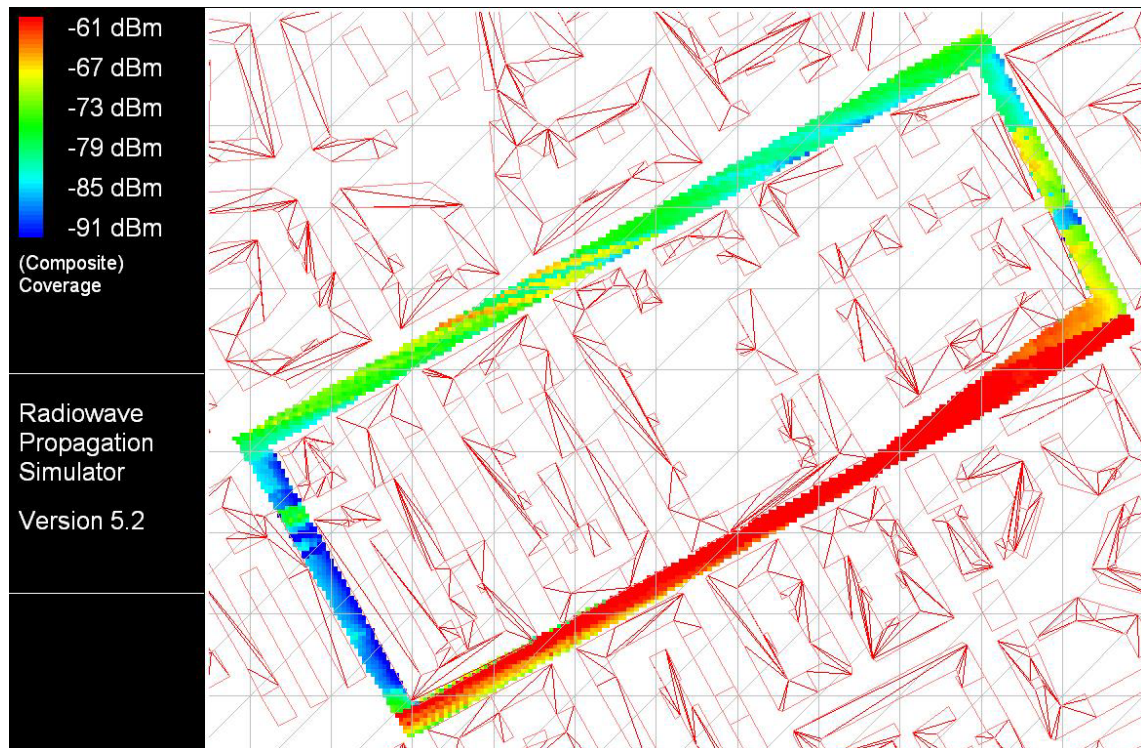


Figure 4.6. Result for the 394 MHz WI-simulation. The colour scale of the power corresponds to that of the measurement.

# Chapter 5 Scenario Aerostat

The scenario exemplifies communications with rescue forces operating within a major city in a crisis situation where the civilian communication infrastructure has been knocked out. The communication system is based on a TETRA base station placed in an aerostat to get coverage. Coverage calculations for this kind of system have been performed with central Stockholm as a test area, [Lundborg *et al.*, 2004]. The simulations were made with RPS 5.2 and rpe.dll from July 2004.

## 5.1. Description of the scenario

The transmitter power for a TETRA base station typically lies in the range of 10 to 40 W, where the lower value would seem realistic for an aerostat. The power at the terminal side is typically 3 W for a vehicle mounted terminal and 1 W for a hand held terminal. Receiver sensitivity at rest is nominally  $-115$  dBm for the base station and  $-112$  dBm for the terminal. During movement these figures are expected to deteriorate by 9 dB, to  $-106$  dBm for the base station and  $-103$  dBm for the terminal. Hence, the base station has a power advantage of 5 to 15 dB, but only 3 dB at reception. As a conclusion, the terminal will hear better than it is heard.

We choose the following parameters for our calculations. They correspond to the downlink with the mobile at rest.

Frequency:	400 MHz
Power:	10 W (base station)
Receiver sensitivity:	$-112$ dBm (mobile)
Antennas:	Isotropic

### Base station

The base station is placed over a large open area, Gärde, immediately to the east of central Stockholm. We have chosen a position with coordinates  $x = 1631.25$  km and  $y = 6581.75$  km in the Swedish map data base RT90; see Figure 5.1. The terrain height according to the terrain data base is there 4.2 m.

Calculations are performed for three different base station antenna heights over ground:

- Mounted on ground vehicle with the antenna at height 3 m.
- Installed in aerostat at height 300 m.
- Installed in aerostat at height 1200 m.

The first case with the base station close to ground is included for reference.

### Terminals

The rescue units move along the streets in central Stockholm. For these we assume the antenna height 3 m. Reception is calculated for a grid of points covering the whole calculation area.



**Figure 5.1. Central Stockholm with the base station (red star) located in the middle of the open field Gårdet.**

### Building data base

The area of the wave propagation calculations is defined by the building data base made available to us through Metria. It covers the northern half of central Stockholm, about  $5.5 \times 3.5$  km according to Figure 5.1. The buildings are placed on top of the terrain height data base RT90.

In the calculations with RPS, vegetation attenuation and penetration into buildings have been neglected. Only three different materials are used with the following real and imaginary parts of the dielectric permittivity:

Building walls (concrete):  $\epsilon_r = 5$ ,  $\epsilon_i = -0.089$

Building roofs (brick):  $\epsilon_r = 4$ ,  $\epsilon_i = -0.16$

Ground (asphalt):  $\epsilon_r = 15$ ,  $\epsilon_i = -15$

The result of this kind of calculation is very sensitive to the settings of the parameters of the program. If detailed description of the field in a particular area is of essence, a number of calculations should be done where the precise locations of the antennas are varied over a small area. Different values of the density of the ray tubes and number of reflections should also be tested. The accuracy of the data bases and the knowledge of material and ground parameters are, of course, also important.

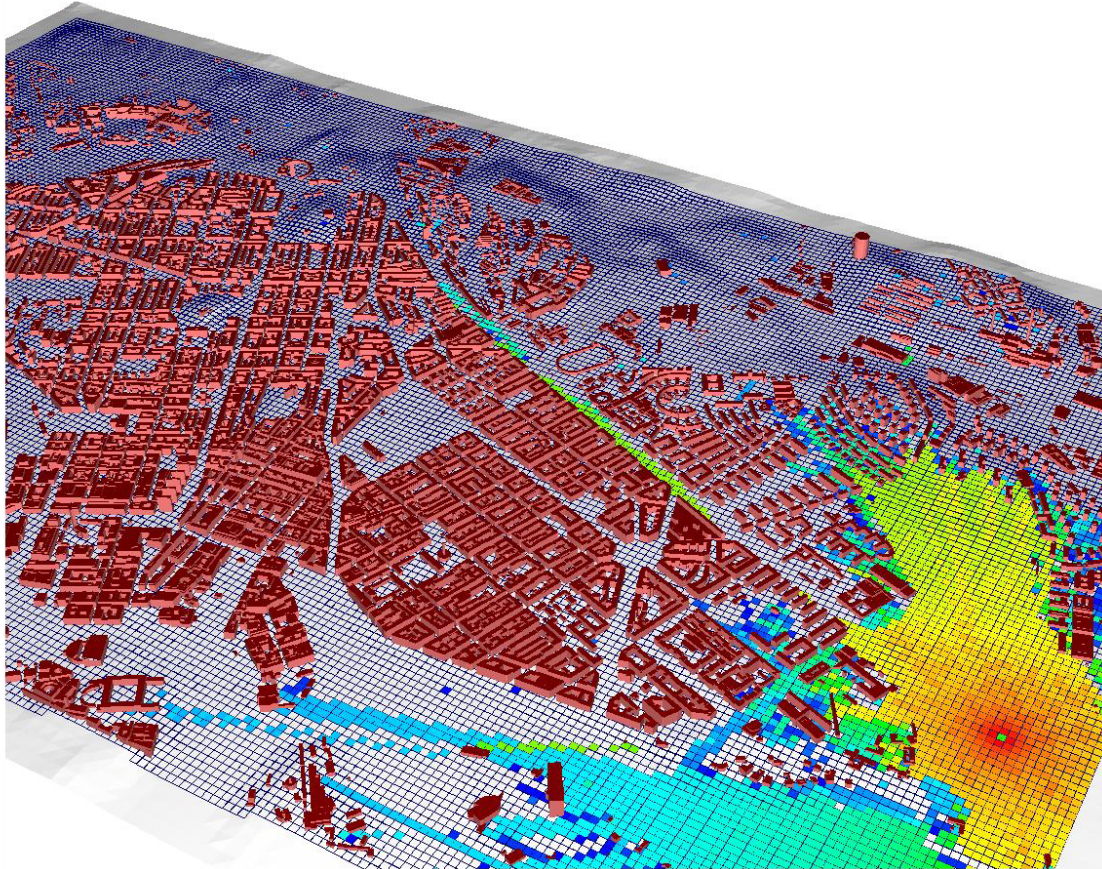
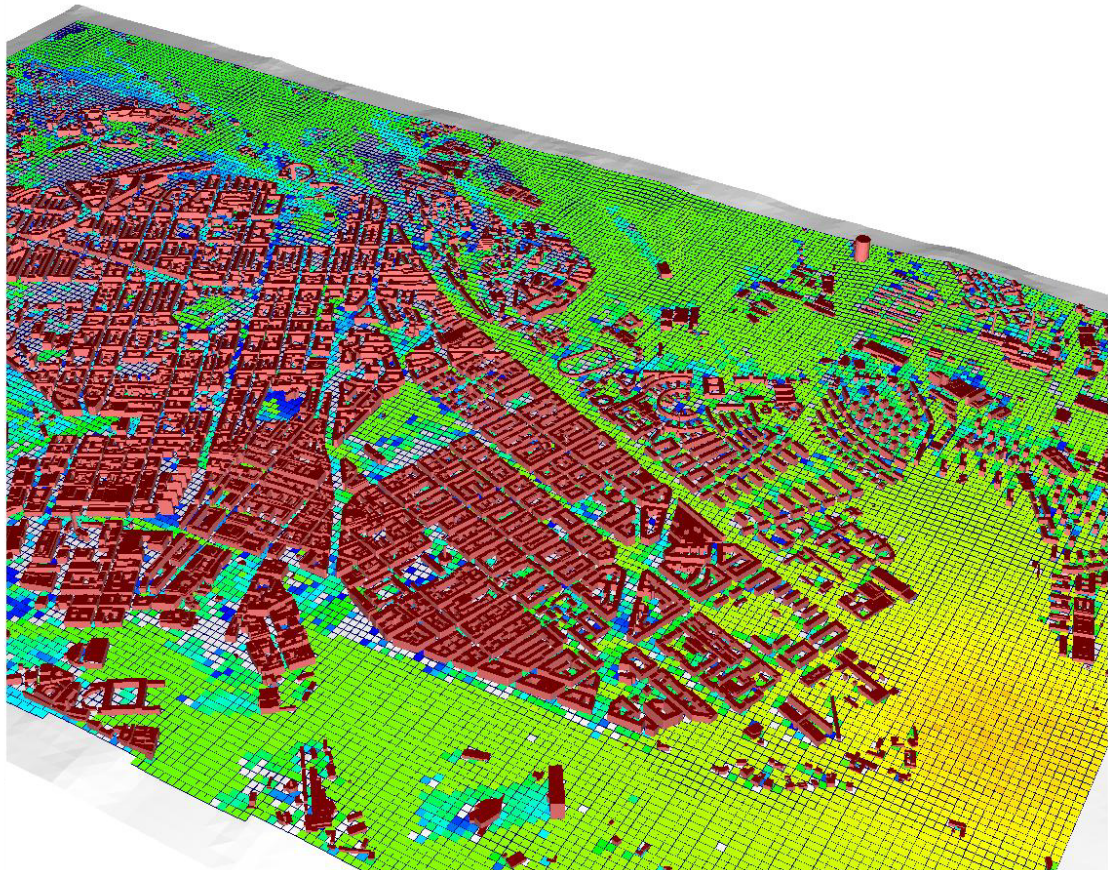


Figure 5.2. Coverage map with the receiver antennas at 3 m height and a transmitting base station placed at Gårdet. The transmitter antenna is vehicle mounted at 3 m height. Colour coding is signal strength according to the scale to the right. White areas on the map implies no coverage, i.e. the signal is below the threshold  $-112 \text{ dBm}$ .



## 5.2. Results of the calculations

As a reference case we made a first calculation with the base station antenna mounted on a ground vehicle. The result of this is presented in Figure 5.2. The picture shows that coverage is good over the areas Gårdet and Djurgården, but the signals are rapidly attenuated in most directions and do not reach more than a couple of houses into the build up areas. The main exception is Valhallavägen, which runs more or less along the sight line from the base station.



**Figure 5.3.** Coverage map with the base station placed at Gärde. The transmitter antenna is aerostat mounted at 300 m height. Signal strength is colour coded as in Figure 5.2.

The situation is dramatically improved by elevating the base station antenna as is clear from Figure 5.3 and Figure 5.4.

With 300 m antenna height (Figure 5.3) coverage is obtained to most of the open areas in the inner city, in particular to hills like, e.g., Observatorielunden. The coverage is incomplete in shadow zones near houses that block the direction towards the base station. This is true, in particular, on streets running at right angles with the main ray direction. Even along such broad roads as Sveavägen or Birger Jarlsgatan coverage is imperfect, because their direction is somewhat unfavourable.

With 1200 m antenna height (Figure 5.4) the situation is further improved. Coverage fails only very close to houses shadowing the direction towards the base station.

These results – with the very large number of buildings and receiver grid points involved – give a good overview of the coverage in the entire area. However, they underestimate the signal level in shadowed areas because of unfavourable settings of the RPS calculations. A discussion of this is found in the next section. It has not been possible, within the time available, to repeat these calculations with better settings.

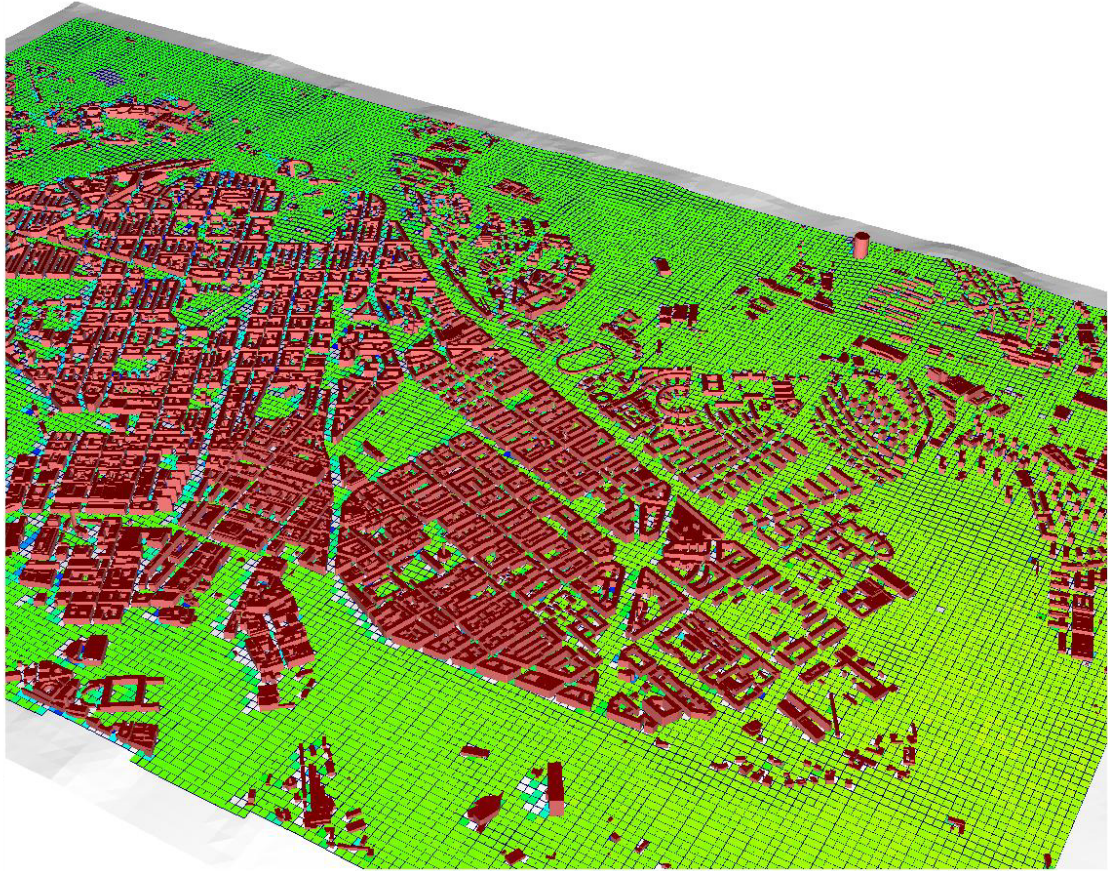


Figure 5.4. Coverage map with the base station placed at Gärde. The transmitter antenna is aerostat mounted at 1200 m height. Signal strength is colour coded as in Figure 5.2 and Figure 5.3.

### 5.3. Discussion

Let us perform a simple 2D geometry consideration to compare the above results with the condition for free optical view towards the base station antenna; see Figure 5.5. We assume for simplicity completely flat ground and that the receiver is at ground level at 3 km distance from the base station. We place a 15 m high obstacle between the base station and the receiver. With 300 m transmitter antenna height this obstacle will block the optical path if it lies closer than 150 m to the receiver. With 1200 m height the obstacle must be closer than 37.5 m to obscure the direct path. With the lowest antenna height of 3 m there is no optical illumination of the receiver at any distance. With this consideration it does not seem unreasonable that coverage may be occasionally lost at road level also for highly elevated aerostats.

At radio frequencies diffraction should improve the situation. Let us consider a similar simple scenario as in Figure 5.5, with an obstacle in the form of a 15 m high and 10 m wide house approximated by a rectangle between the terminals. In this case the distance between the base station and the right wall of the house is 3 km. The receiver antenna height is 3 m. Figure 5.6 shows the calculated received signal power as function of the receiver distance from the house when diffraction is included. This result was produced with a higher-order GTD (geometrical theory of diffraction) implementation separate from RPS.

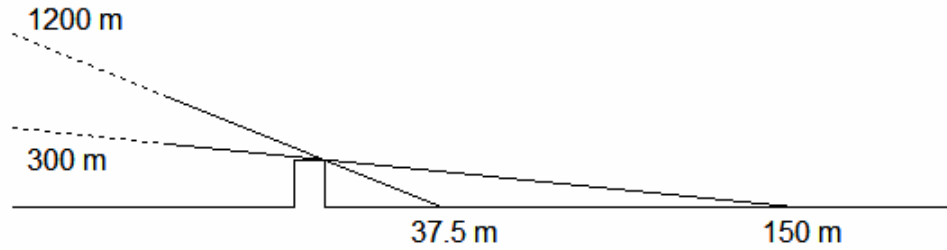


Figure 5.5. Shadow zone (at ground level) behind a 15 m high house for the two aerostat cases.

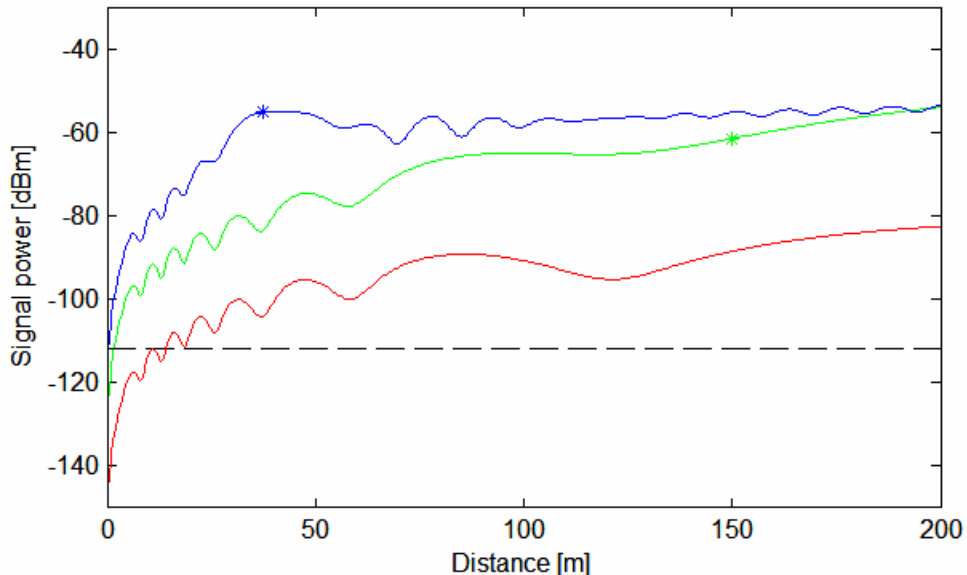
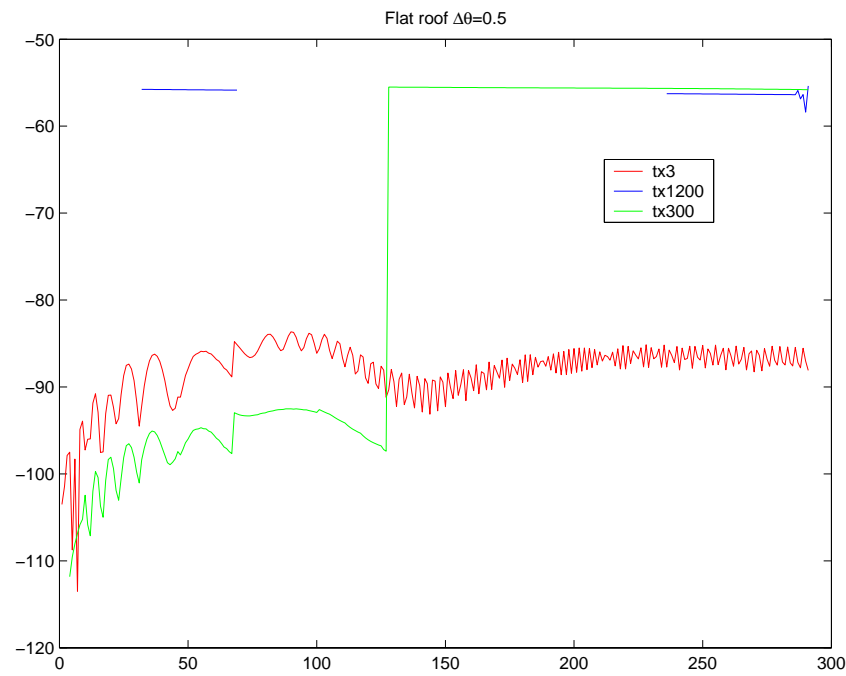


Figure 5.6. Signal level [dBm] as a function of the distance between the receiver and the house for the three transmitter antenna heights considered 3 m (red), 300 m (green) and 1200 m (blue). The base station power is 10 W and it is located 3 km from the house. The stars on the upper two curves are put at the respective shadow zone distances. Calculation was done with higher-order GTD.

The same geometry generated for RPS gives the result in Figure 5.7. First we notice that many rays are missing in the 1200 m (blue) case where the receiver points are directly illuminated; this was found out to be a flaw in the program, but it is corrected with the rpe.dll dated 2004-08-24. Secondly, the signal drops much too sharply into the shadow region. The highest angle of incidence drops fastest, in contrast to physics and Figure 5.6. The reason for the totally missing diffraction over the building for the highest transmitter is that the ray launching implementation in RPS fails to find the diffraction edge. There will be a too large spacing between adjacent rays when the travelled ray distance is too high. The problem can be solved by using much smaller steps in elevation, but for the scenarios we have described in the report this will give much higher simulation times. The reason why the middle transmitter has lower signal power near the building than the lowest transmitter is that the ray is reflected in the ground and after that it hits both the diffraction edges of the building, which gives a higher reduction of the signal strength.

Figure 5.8 shows the result of a similar calculation where the cross-section of the house is changed from a rectangle to a triangle, so as to reduce the problem to single diffraction. The triangle has base 10 m and height 15 m. The missing parts should disappear if the simulation is re-run with the updated version of the software.



**Figure 5.7.** Diffraction over the rectangular building described above, calculated with RPS.

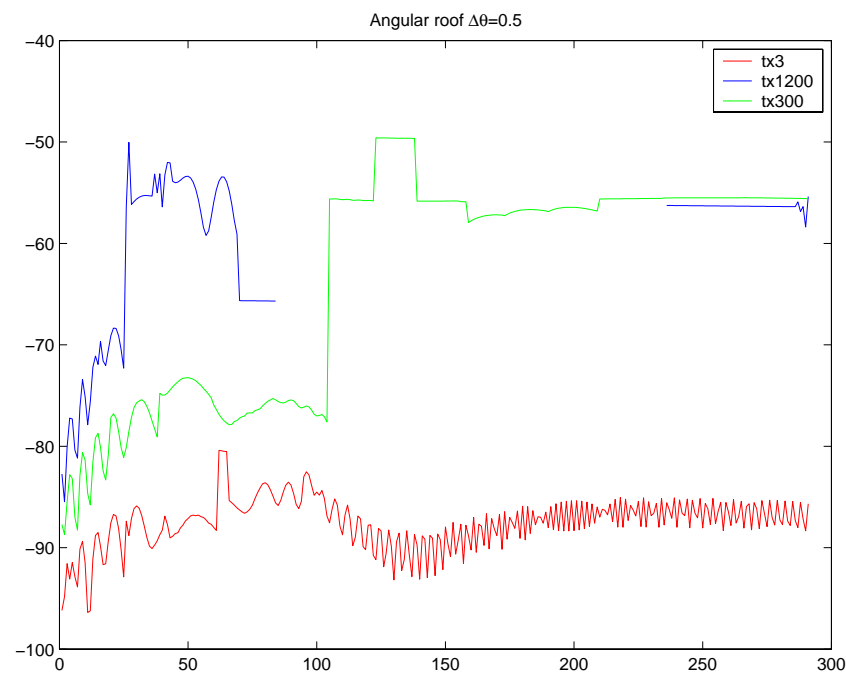


**Figure 5.8.** Diffraction over a triangular building, calculated with RPS.

# Chapter 6 Conclusions

Calculating the wave propagation in built-up areas can be very complicated due to the environment and the requirements on the results. Exact results are difficult to achieve since the map database has a limited resolution. Our databases have a resolution of 50 m in the underlying terrain and perhaps one metre in the building details and in propagation calculations that is fairly rough.

Also buildings, trees in parks, lampposts, traffic signs and vehicles affect the wave propagation. These objects are most certainly not included in the building database. If they were, they should also be described by appropriate material parameters. How the results are depending on the values of the material parameters is not sorted out. It would be of interest to investigate that dependency.

In this report, we have described some problems with the calculations with RPS. Although some of the problems are not yet solved, there is a great advantage to acquire commercial software that allows custom plug-ins. Mostly because one thereby avoid the time consuming programming of the algorithms and the user interfaces. Also the validation of an advanced software will require large efforts. It is, though, important to state that no such computer software is trivial to use. Prepare for an extensive learning period, some problems with the computations and maybe also with the relevance of the results. In the case of RPS, we wish to mention the excellent help and support from Radioplan in problem solving.

## 6.1. Future Work

### RPS algorithms

There is still a lot of work to be done in testing the software to determine which settings give the best results, taking the simulation time as one of the decision parameters. Some issues need to be further clarified with the RPS manufacturer. One of these is the signal to interference ratio calculation when transmitters use slightly different frequencies with overlapping pass bands. What is the algorithm for this? A second issue is the calculation of angular spread, which may probably go wrong when folding occurs over the interval boundary at  $\pm 180^\circ$ . One further issue is the representation of small-scale fading effects. The static field calculation contains all data necessary to do this, but an interpolation algorithm has to be devised which accounts for the position dependent phases. If this interpolation is done over several adjacent receiver grid points one would also obtain some filtering of the effects of misaligned ray tubes pointed out in section 3.6.

Tests on how the change of material properties affects the simulation results are also of great interest. There is a need also in getting material properties for other frequencies than the band between 900 MHz – 2 GHz and around 60 GHz. Ideally, this can be done through literature studies, but published data seems to be incomplete. Hence measurements are probably needed.

RPS is developed for wave propagation calculations in the frequency range 300 MHz to 300 GHz. Military radio systems use even lower frequencies and to extend the frequency range down to 50 MHz would be of interest.

In the project KOMET we have access to a RUSK measurement system. It is a MIMO-channel sounder which is unique, since it has the ability to make measurements in the 300 MHz band, as well as in the commercial communication bands of 2.4 and 5.4 GHz. We will use the RPS software for comparisons with measurements made with the RUSK system [Waern *et al.*, 2004].

In another project at the department of sensor technology a technique is developed of laser scanning the environment [Ahlberg *et al.*, 2003]. It is clearly a very comprehensive task to produce such data. An interesting prospect, nevertheless, is to investigate the possibility to use these measurements as input for the building database. If this works it could be of importance when doing calculations for environments where no building database is available, e.g. in international scenarios.

## Scenarios

There are many types of scenarios that would be of interest for further investigations.

For example:

- Road crossings with a lot of transmitters in a very small area.
- Operations inside a building with communication between different rooms, floors and to the outside (i.e. outdoor to indoor communication), without having any communication infrastructure.
- Find out whether it is possible to use the software for simulation of communication in tunnels. Is ray tracing usable for this or should other techniques such as PE, Parabolic Equations, be used for this type of scenario?

## Extensions of RPS

As an alternative to the Walfisch-Ikegami model, making an implementation of the Okumura-Hata model could also be of interest for rapid calculations.

In this respect RPS has a particular advantage since different model algorithms can be made available to us, if needed. Furthermore, Radioplan themselves are also interested in developing their software after user requirements.

# Chapter 7 References

- RPS Radiowave Propagation Simulator*, User Manual-Version 5.1, Radioplan GmbH, Dresden, 2003.
- RPS Radiowave Propagation Simulator*, User Manual-Version 5.2, Radioplan GmbH, Dresden, 2004.
- S. Ahlberg, M. Elmquist, Å. Persson, U. Söderman, "Metoder för framställning av högupplösta syntetiska omgivningar/omvärldsmodeller för sensorsimulering", FOI, Linköping, FOI-R--1110--SE, 2003.
- L. Barclay (Ed.), *Propagation of Radiowaves*, 2nd edition, Institution of Electrical Engineers, London 2003.
- N. Blaunstein and M. Levin, "VHF/UHF wave attenuation in a city with regularly spaced buildings," *Radio Science*, vol. 31, no. 2, pp. 313-323, March-April 1996.
- Å. Blomquist, F. Eklund, R. Lindquist, K. Engström, L. Ericson, "Radiovågors utbredning. Jordytans inverkan. Kap 5-6." FOA, Stockholm, FOA kompendium nr 24 A, 1969.
- M. F. Cátedra, J. Pérez-Arriaga, *Cell planning for wireless communications*, Artech, Boston, MA, 1999.
- D. C. Cox, "Delay Doppler characteristics of multipath propagation at 910 MHz in a suburban mobile radio environment.", *IEEE Trans. Antennas Propagat.*, vol. 20, No 5, pp 625-635, 1972.
- L. Juan-Llácer and N. Cardona, "UTD solution for the multiple building diffraction attenuation function for mobile radiowave propagation," *Electron. Lett.*, vol. 33, no. 1, pp. 92-93, Jan. 1997.
- G. Gustafsson, "Radiotäckningsmätningar i Stockholm", AerotechTelub K2-02:1436, 2002 (can bee found at [Gustafsson and Ladell, 2002]).
- G. Gustafsson, L. Ladell, "Vågutbredningsmätningar i Stockholm", (CD), AerotechTelub K2-02:1918, FOI Dnr 02-1111:12, 2002.
- P. Holm, L. Ladell, "Smalbandiga mätningar i Stockholm – sammanställning av resultat" (Draft, 2004).
- A. G. Kanatas, I. D. Kountouris, G. B. Kostaras, and P. Constantinou, "A UTD propagation model in urban microcellular environments," *IEEE Trans. Antennas Propagat.*, vol. 46, no. 1, pp. 185-193, Feb. 1997.
- B. Lundborg, L. Ladell, "Three-dimensional radiation pattern for antennas with one-dimensional current distribution." *Proc. Antenn 03, Kalmar, Sweden*, pp. 321-326, 2003.
- B. Lundborg, L. Ladell, K. Persson, E. Löfsved, "Aerostatstudie kommunikation – Beräkningsfall", AerotechTelub K4-04:0139, FOI Memo 976, Sep. 2004.
- B. Lundborg, O. Tronarp, "Första utvärdering av RPS", FOI Dnr 03-2966:1, Dec. 2003.
- D. A. McNamara, C. W. I. Pistorius, and J. A. G. Malherbe, *Introduction to the Uniform Geometrical Theory of Diffraction*, Artech House, Norwood, MA, 1990.
- M. J. Neve and G. B. Rowe, "Contributions towards the development of a UTD-based model for cellular radio propagation prediction," *IEE Proc.-Microw. Antennas Propagat.*, vol. 141, no. 5, pp. 407-414, Oct. 1994.

- S. R. Saunders and F. R. Bonar, "Explicit multiple building diffraction attenuation function for mobile radio wave propagation," *Electron. Lett.*, vol. 27, no. 14, pp. 1276-1277, July 1991.
- M. Stenström, G. Eriksson, L. Ladell, "Impulssvarsmätningar", (CD), AerotechTelub K2-01:0376, FOI Dnr 01-2142:9.
- S. Y. Tan and H. S. Tan, "A microcellular communications propagation model based on the uniform theory of diffraction and multiple image theory," *IEEE Trans. Antennas Propagat.*, vol. 44, no. 10, pp. 1317-1326, Oct. 1996.
- J. Walfisch and H. L. Bertoni, "A theoretical model of UHF propagation in urban environments," *IEEE Trans. Antennas Propagat.*, vol. 36, no. 12, pp. 1788-1796, Dec. 1988.
- Å. Waern, B. Lundborg, G. Eriksson, M. Alexandersson, "Kommunikationskanalen i urban miljö - beskrivning av MIMO-konceptet och RUSK kanalsond," FOI, Linköping, FOI-R—1200—SE, June 2004.

# Appendix A Export of data

In this appendix some of the data export options are described. The titles used for the subsections are directly taken from the export command in RPS.

## Export received power and delay spread

This export option generates a quite small ASCII-file in txt-format containing some general information, such as numbers of receivers (dataset records), centre frequency and bandwidth. Each row in the result matrix contains the result for one receiver and the columns contain data as described in the table below.

Column	Contains
1	Receiver position, x, [m]
2	Receiver position, y, [m]
3	Receiver position, z, [m]
4	Total received power [dB/dBm]
5	Delay spread [ns]
6+(2n-1)	Power from transmitter “name of transmitter”
7+(2n-1)	Delay spread from transmitter “name of transmitter”

n = number of transmitters.

## Data as ASCII file

This export option generates an ASCII-file in txt-format. It starts with some general information such as numbers of receivers (dataset records) and centre frequency. Data is then presented for each of the receivers, i.e. there is one matrix with all rays contributing to each of the receivers. Since all ray contributions with their own delays are saved this implies that the bandwidth is infinite. Each row in the result matrix contains the contribution to the specified receiver of one ray. The columns contain data as described in the table below.

Column	Contains
1	Name of the transmitter generating the received ray.
2	Delay, TAU [ns]
3	Magnitude [dB/dBm]
4	Phase [°]
5	Azimuth (PHI) at transmitter [°]
6	Elevation (THETA) at transmitter [°]
7	Azimuth (PHI) at receiver [°]
8	Elevation (THETA) at receiver [°]

## Export DOA as ASCII file

This export option generates an ASCII-file in txt-format. It starts with some general information such as numbers of receivers (dataset records) and centre frequency. Data is then presented for each of the receivers, i.e. there is one matrix with all rays contributing to each of the receivers. Since all ray contributions with their own delays are saved this implies that the bandwidth is infinite. Each row in the result matrix contains the contribution to the specified receiver of one ray. The columns contain data as described in the table below.

Column	Contains
1	Azimuth (PHI) [ $^{\circ}$ ] referring to the receiver for the values in column 2 and to the transmitter for the values in column 3. (The integer part of the value is used.)
2	Power at the receiver [dB/dBm]
3	Power at the transmitter (uplink) [dB/dBm]

## Export static data as matrices readable with Matlab

Running the export option “Export dynamic data as matrices readable with Matlab” generates a \*.mat file including the following parameters.

RPS_Bandwidth	Bandwidth in GHz.
RPS_CenterFrequency	Centre frequency in GHz.
RPS_Magnitude	A sparse matrix containing the complex impulse response. [V]
RPS_NoiseFloor	[dB]
RPS_NumResolvablePaths	Number of resolvable paths at each receiver
RPS_Rx_PHI	Azimuth at the receiver for each “ray” in the IR
RPS_Rx_Position	Receiver positions x, y, z in m
RPS_Rx_THETA	Elevation at the receiver for each “ray” in the IR
RPS_Tx_Names	List of names of the transmitters
RPS_Tx_PHI	Azimuth at the transmitter for each “ray” in the IR
RPS_Tx_Position	Position for the transmitters x, y, z [m]
RPS_Tx_THETA	Elevation at the transmitter for each “ray” in the IR

The delay steps are determined from the bandwidth of the simulation. The number of delays is given by the maximum delay and the delay step as follows:

$$\Delta\tau = 1/B$$

$$N_{\text{del}} = \tau_{\max} / \Delta\tau$$

At the transmitter and the receiver, the angle for the rays is given as looking outwards from the respective antenna. This means that the k-vector at the receiver has opposite direction as compared to the presented angles.

## Export dynamic data as matrices readable with Matlab

Name	Size	
RPS_ActiveTxID	Step x 1	Gives the active transmitter ID for each time step. Only one transmitter can be active at each step.
RPS_Bandwidth	1x1	Bandwidth [GHz]
RPS_CenterFrequency	1x1	Centerfrequency [GHz]
RPS_Magnitude	Step x delays	The complex impulse response for each time step [V]
RPS_NoiseFloor	1x1	[dB]
RPS_NormalizeExcessDelay	1x1	0=Absolute delay 1=Excess delay. The delay of the first path is normalized to 0s.
RPS_NormalizePower	1x1	0=No normalisation of the power. 1=The power of each impulse response is normalized such that its square sum is equal to 1
RPS_NumResolvablePaths	Step x 1	Number of resolvable paths for each time step.
RPS_Rx_PHI	Step x delays	Azimuth at the receiver for each delay in the IR
RPS_Rx_Position	Step x 3	
RPS_Rx_THETA	Step x delays	Elevation at the receiver for each delay in the IR
RPS_TimeInterval	1x1	
RPS_Tx_Names	Number of transmitters	List of names of the transmitters
RPS_Tx_PHI	Step x delays	Azimuth at the transmitter for each delay in the IR
RPS_Tx_Position	Number of transmitters x 3	Position for the transmitters x, y, z [m]
RPS_Tx_THETA	Step x delays	Elevation at the transmitter for each delay in the IR
RPS_Velocity	1x1	

The delay step is determined from the bandwidth, either the value used in the simulation or an input given when exporting the result. The number of delays is given as an input:

$$\Delta\tau = 1/B$$

$$\tau_{\max} = N_{\text{del}} \cdot \Delta\tau$$

## Appendix B. Narrowband results, Stockholm

All the figures in Appendix B are from the scenario described in Section 4.2.

The following pages with figures are organised with one page per frequency and the three figures on each page in the following order:

- |                |                                     |
|----------------|-------------------------------------|
| At the top:    | Measurement                         |
| In the middle: | 3D-ray tracing                      |
| At the bottom: | COST 231-Walfisch-Ikegami model, WI |

When comparing the figures it is important to remember that they have different colour scales. The scale for each frequency of the measurement spans maximum to minimum received power averaged over a distance of 10 m. The scale for each frequency for the ray-tracing simulation spans maximum to minimum received calculated power. For the WI model the scale is roughly the same as for the measurement for that particular frequency. Hence, for each frequency the measurement and the WI-model have the same scales but the ray tracing simulation has a different scale.

### Measurements

Starting with the measurements, the most general observation is that the power decreases with increasing frequency over the entire receiver area. The variation of the signal strength along the sections of the measurement route is rather different depending on frequency.

This is particularly obvious if one compares the highest and lowest frequencies shown in figures B.5 and B.1. For the lowest frequency the west corner of the lower long side has the highest loss, but for the highest frequency the loss at this section is the smallest; the difference is there only about 10 dB. Looking instead at the midsection of the upper long side, the signal strength for the lowest frequency is found to have its maximum here, which is about -55 dBm. For the highest frequency this section has very poor signal strengths, only about -110 dBm, and thus the difference is there about 55 dB.

### Ray tracing

The results from the 3D ray tracing simulations are presented in the middle in each set of figures. The settings used for the simulations are described in Section 4.2.1. These were the only settings used for the simulation and we are not at all certain that they are optimal. However, they gave acceptable simulation times, in the range between 5 hours and 3 days. Setting the step size in azimuth and elevation much smaller than this would result in much more rays to be accounted for and thus much longer simulation times. The only setting changed when shifting to a new frequency was the receiver sensitivity, the noise floor. This had to be done in order to keep simulation time down, as the power loss is much smaller for low frequencies than for high frequencies.

When comparing the ray tracing simulation against each other one can see that for all simulations, except possibly for the case 394 MHz shown in figure B.3, there is a stronger sharp trail along the lower long side. We have not been able to determine what causes this trail. One can also see that the highest signal strength decreases with higher frequency, which was expected. The gap at the right short side shows that the signal strength at this section of the route is less

than the noise floor for (almost) all frequencies. It also indicates that there might be a problem with finding the diffraction edges for the ray tracing algorithm. This might be solved by using other settings, especially for the step size in elevation, or by setting simple over rooftop diffraction, but this has not been investigated.

The best agreement between measurement and ray tracing is found for the highest frequencies. This is also the range for which RPS was designed. In the simulation at 394 MHz, Figure B.3, some of the receivers have powers in the same range as the corresponding ones in the measurement. But most of the receivers have much lower powers, by approximately 15 dB. Apart from the level, the fading patterns from the simulation show a fair similarity to the measurements.

In Figure B.4 for 915.5 MHz the simulation shows quite a decent image of the fading pattern. The simulation is of the order of 15 dB lower than the measurement. Also for the frequency 1794 MHz, Figure B.5, the simulation gives a rather good image of the fading pattern, especially in the upper right region and in the lower left region. The difference in level is about 15 dB for this frequency too.

The lower frequencies, Figure B.1 for 51 MHz and Figure B.2 for 250.5 MHz, are below the design limit of the software and also show poor agreement between simulations and measurements. The simulations fail to reproduce the shift of the strongest signal from the lower long section to the upper one.

The strongest calculated signal at 51 MHz is found in the lower left of the path, where the measurement actually has the lowest signal. The calculation resembles more the measurement results for higher frequencies. Unfortunately there is a gap in the measurement where the simulation has a section of very high signal strength. At some sections of the path the signal strength is overestimated. Nor does the simulation at 250.5 MHz, Figure B.2, show any especially good agreement between simulations and measurements.

## **Walfisch-Ikegami**

Looking at the simulations made with the WI-model one can see that the surface plots are identical for the different frequencies, apart from the differing colour scales. This is expected because of the simple frequency dependence of the WI-model. This simplified model accounts for the propagation loss with respect to free space loss, multiple knife-edge diffraction to the top of the final building and the single diffraction and scattering process down to street level [Barclay, 2003, Section 11.2.4.5].

For the frequencies 394 and 915.5 MHz, in Figure B.4, one can see fairly good agreements between the WI-model and the measurements. Also for the higher frequency 1794 MHz there is a fair agreement between the simulation and the measurement, which can be seen in Figure B.5. For the lower frequencies the agreement is rather bad, the signal strength is too high and the large scale fading patterns disagree. This is no surprise since the WI-model is designed for the frequency range 800 MHz – 2 GHz. (There is a very good agreement in the north-west corner and at the right short side for the lowest frequency, Figure B.1, but this is probably a mere coincidence.)

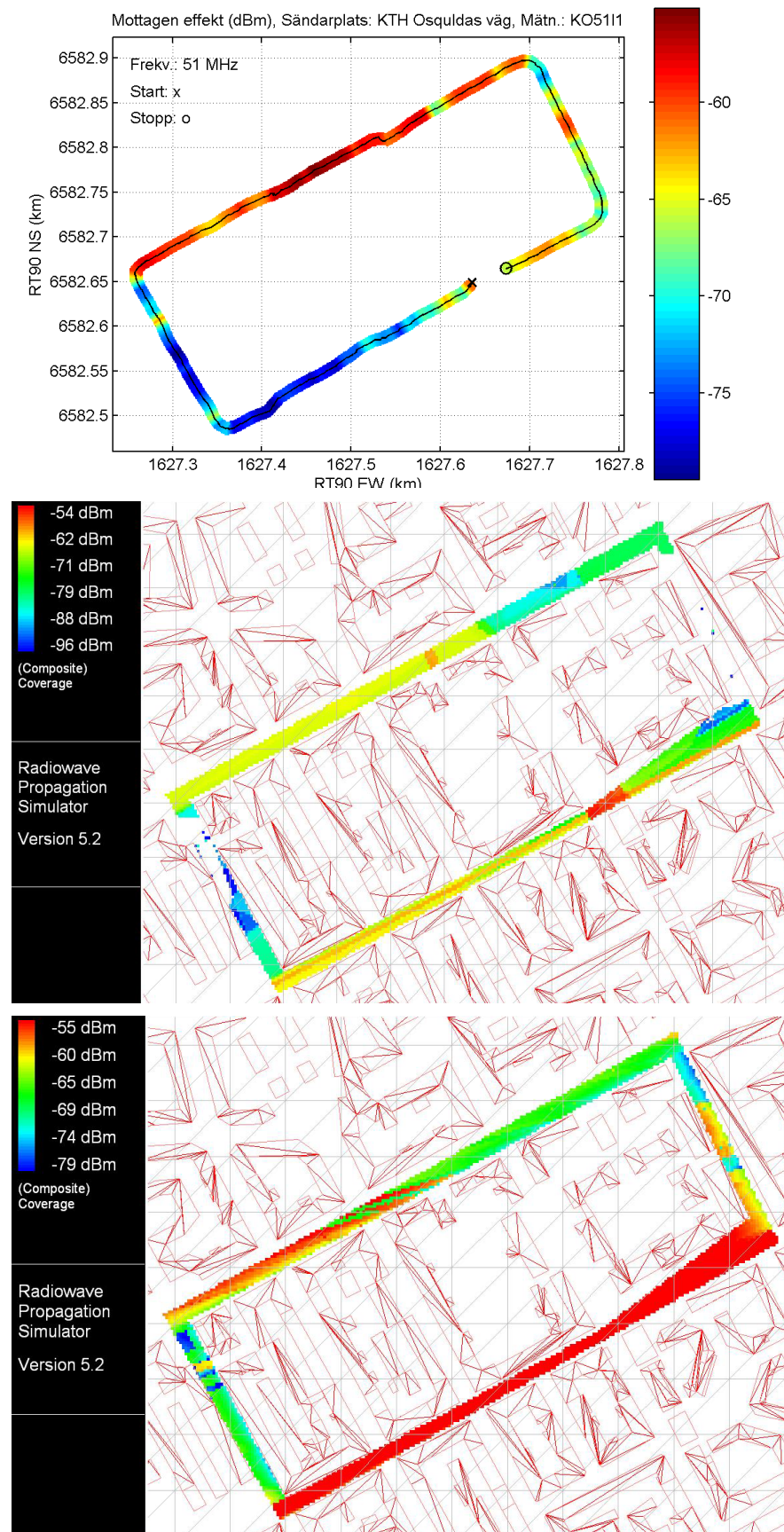


**Figure B.1.** Results for 51 MHz. The figure shows from top to bottom: measurement, 3D-ray tracing simulation and Walfisch-Ikegami simulation.

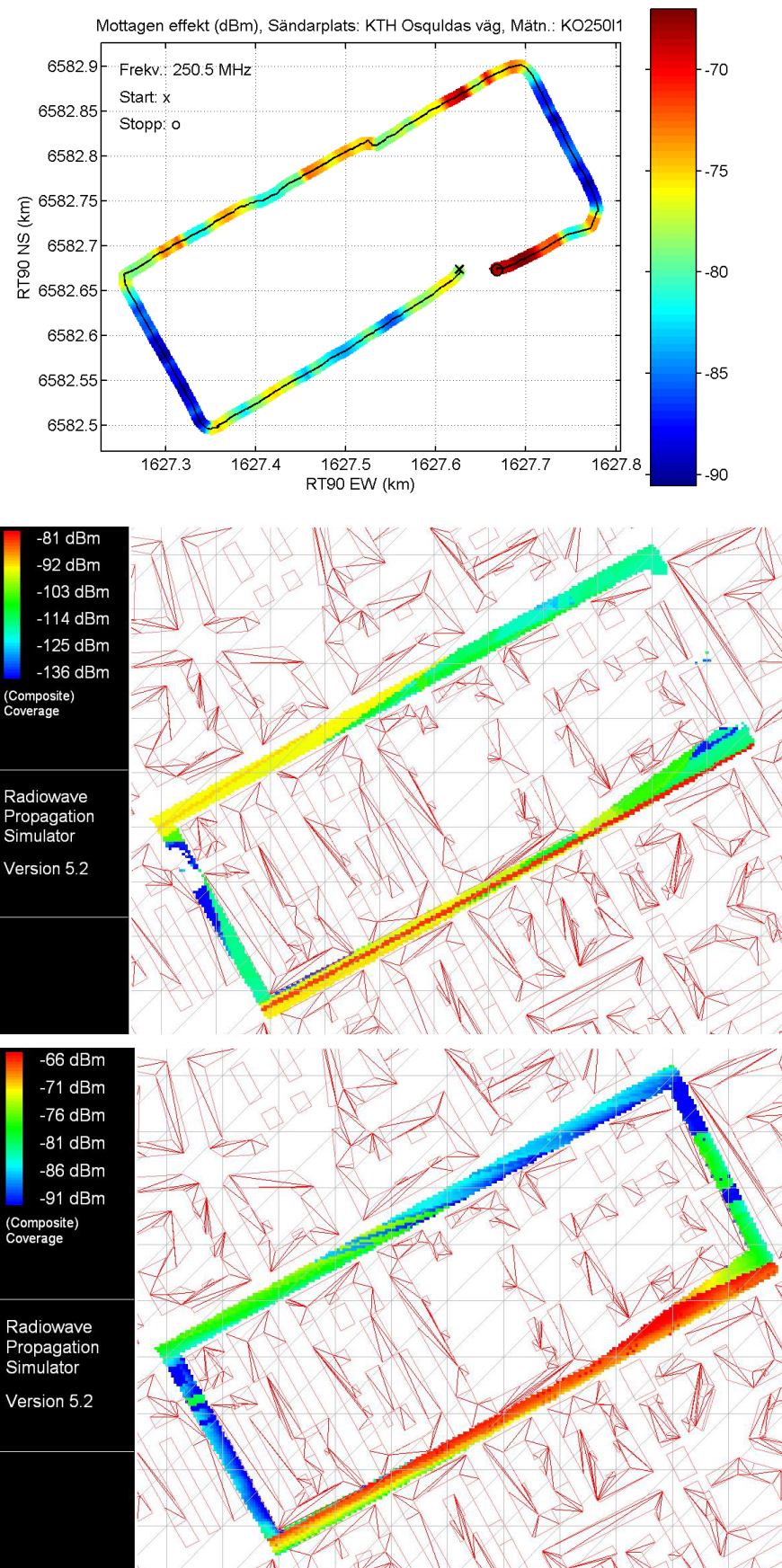


**Figure B.2.** Results for 250.5 MHz. The figure shows from top to bottom: measurement, 3D-ray tracing simulation and Walfisch-Ikegami simulation.

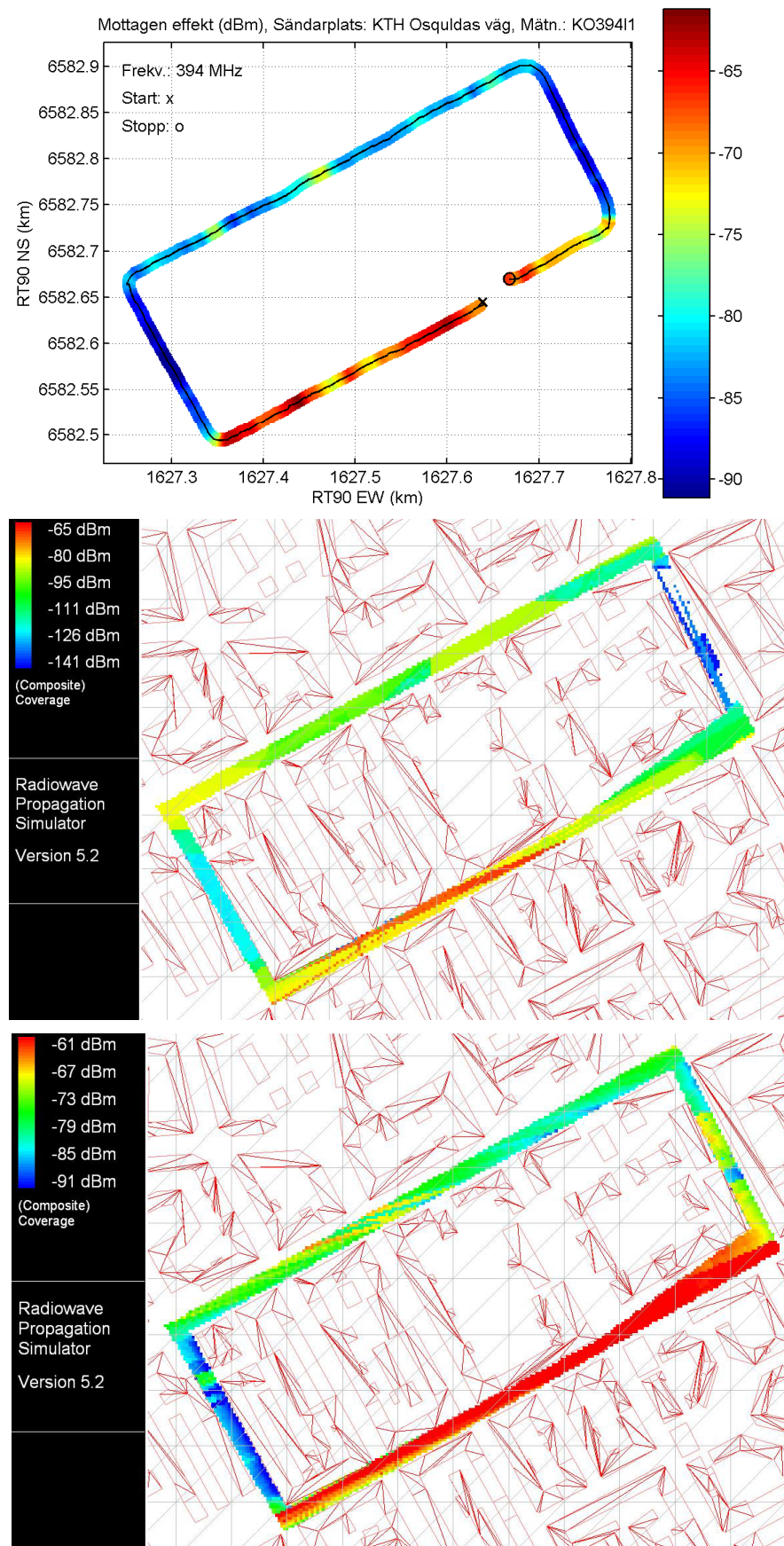


**Figure B.3.** Results for 394 MHz. The figure shows from top to bottom: measurement, 3D-ray tracing simulation and Walfisch-Ikegami simulation.

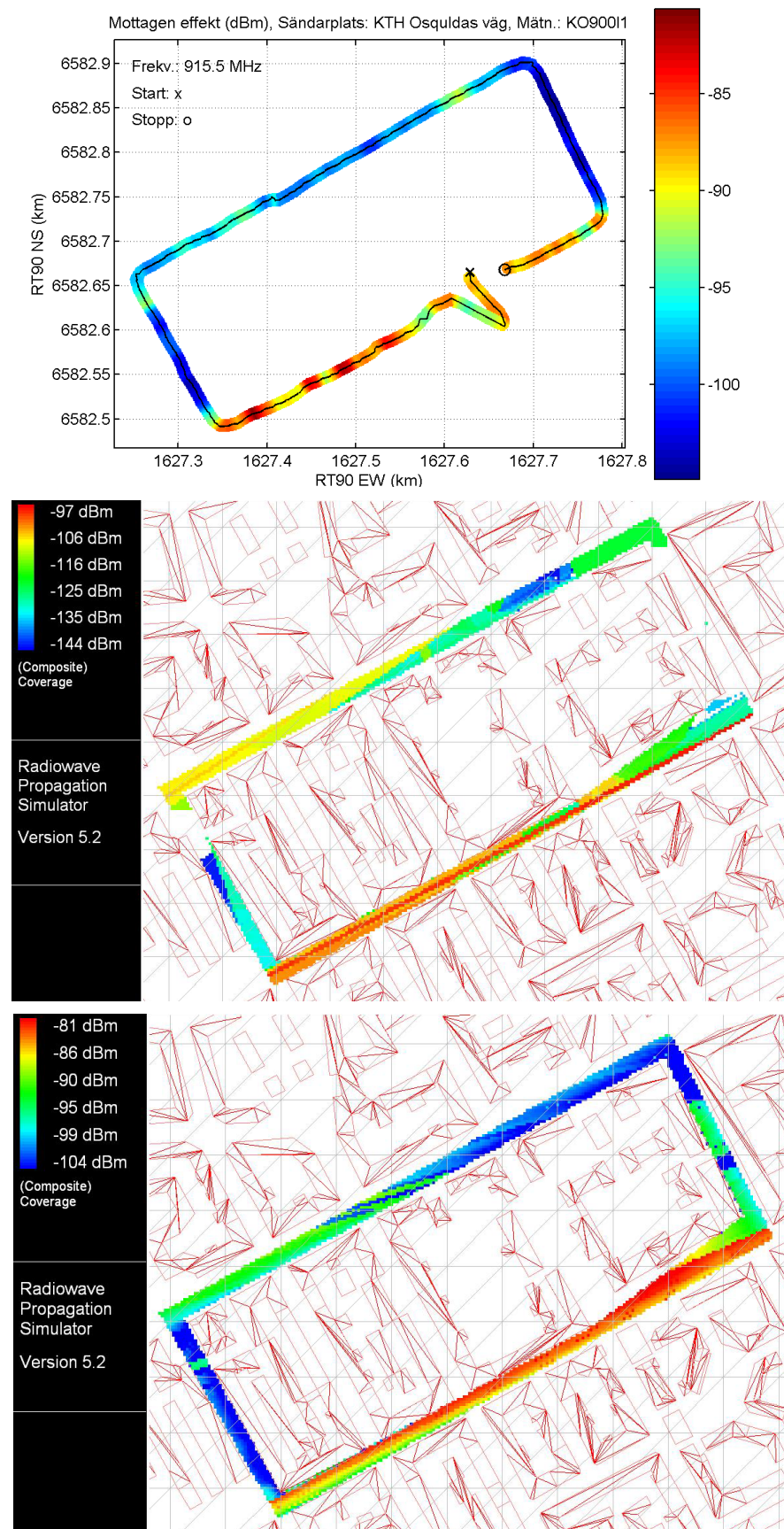
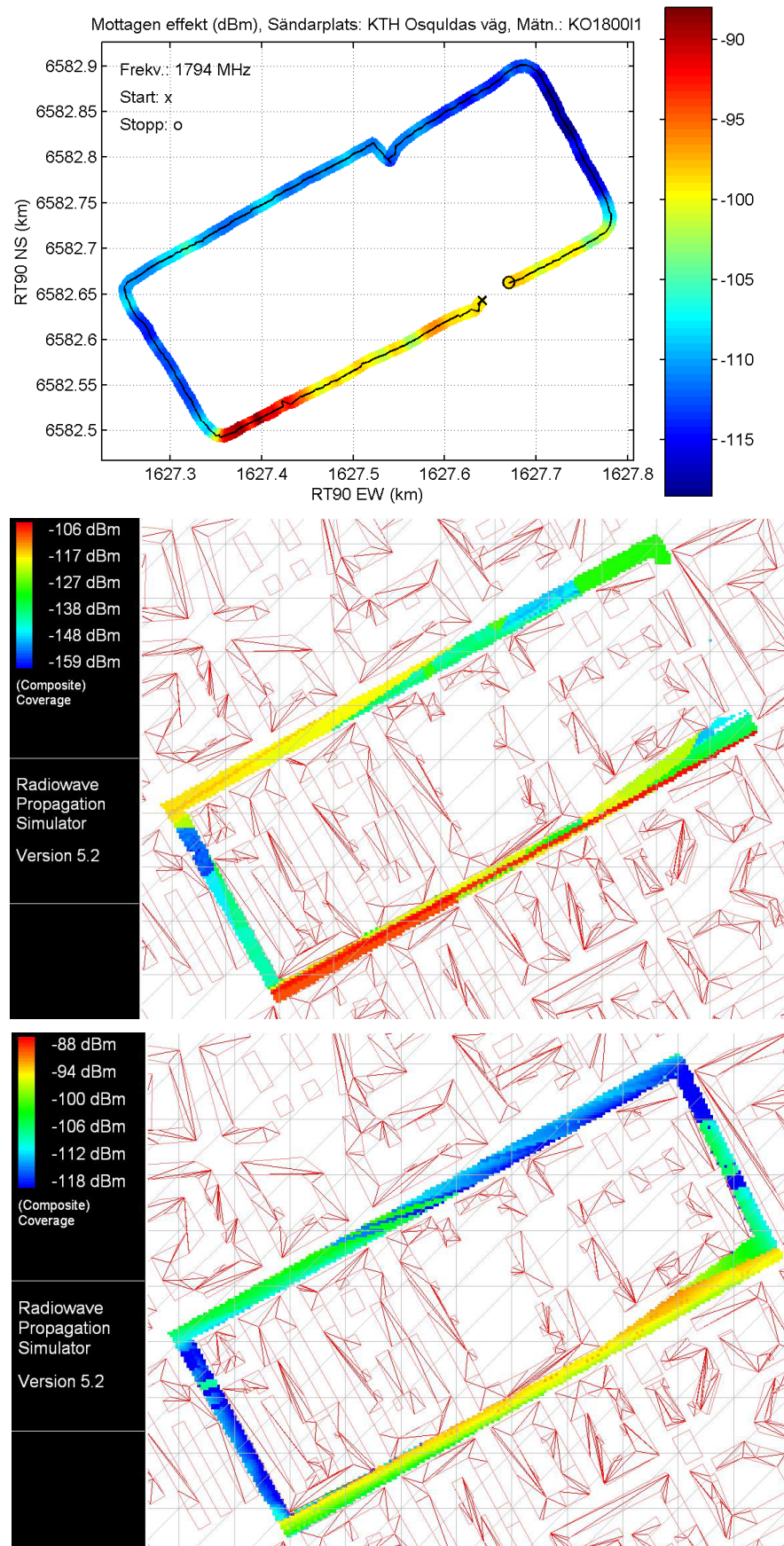


Figure B.4. Results for 915.5 MHz. The figure shows from top to bottom: measurement, 3D-ray tracing simulation and Walfisch-Ikegami simulation.



**Figure B.5.** Results for 1794 MHz. The figure shows from top to bottom: measurement, 3D-ray tracing simulation and Walfisch-Ikegami simulation.